A case-study of the coupled ocean–atmosphere response to an oceanic diurnal warm layer

Pierre-Etienne Brilouet, Jean-Luc Redelsperger, Marie-Noëlle Bouin, Fleur Couvreux, Cindy Lebeaupin Brossier

RESEARCH ARTICLE

A Case Study of the Coupled Ocean-Atmosphere Response to an Oceanic Diurnal Warm Layer

Pierre-Etienne Brilouet[1, 2] | Jean-Luc Redelsperger[1] | Marie-Noëlle Bouin[2, 1] | Fleur Couvreux[2] | Cindy Lebeaupin Brossier[2]

[1]Ifremer, Univ. Brest, CNRS, IRD, Laboratoire d'Océanographie Physique et Spatiale (LOPS), IUEM, Brest 29280, France

[2]CNRM, Université de Toulouse, Météo-France, CNRS, Toulouse, France

Correspondence
Pierre-Etienne Brilouet, Ifremer, Univ. Brest, CNRS, IRD, Laboratoire d'Océanographie Physique et Spatiale (LOPS), IUEM, Brest 29280, France
Email: pierre-etienne.brilouet@aero.obs-mip.fr

Present address
Laboratoire d'Aérologie, University of Toulouse, CNRS, UPS, Toulouse

Funding information
ANR-COCOA (COmprehensive Coupling approach for the Ocean and the Atmosphere), Grant/Award Numbers: ANR-16-CE01-0007

A modelling case study based on observations from the Dynamics of the Madden-Julian Oscillation field campaign is presented and discussed. It aims at investigating the ocean-atmosphere coupling and the marine atmospheric boundary layer structure over an oceanic diurnal warm layer. This case corresponds to the development of a diurnal warm layer characterized by a sea surface temperature diurnal cycle of ~ 2°C. A 1-D oceanic model with high vertical resolution is used to investigate the mechanisms responsible for the establishment and decay of the diurnal warm layer highlighting competing impact of the absorption of the solar radiation, the turbulent transport and the surface heat loss. An atmospheric large-eddy simulation coupled to the 1-D oceanic model is then presented and extensively evaluated against the numerous observations available for this case. The simulation is able to reproduce the surface fluxes and the main boundary layer structures. This study thus provides a case to investigate the ability of parametrizations to handle the ocean-atmosphere coupling and its impact on the atmospheric boundary layer.

KEYWORDS
Diurnal Warm Layer, Ocean-Atmosphere Coupling, Large-Eddy Simulation.

1 | INTRODUCTION

In the tropical regions, the ocean-atmosphere (O-A) interactions happen on a wide range of spatial and temporal scales. Their appropriate representations are fundamental for tropical weather forecasting and climate modelling. The turbulent exchanges of heat and water vapour at the air–sea interface are mainly driven by two parameters, the sea surface temperature (SST) and the surface wind speed (U_0). According to the spatial and temporal scales considered, the variability of the air-sea exchanges appears to be dominated by the SST variability at global or regional scales, while the U_0 variability seems prevalent at meso and local scales. Surface temperature variations at the daily timescale are generally smaller over the ocean (Clayson and Weitlich, 2007) than over a continental surface. However when appropriate conditions for the development of a diurnal warm layer (DWL) are established, an amplitude of the SST diurnal variability up to several degrees can be reached. Under relatively calm near-surface wind conditions leading to a weak oceanic vertical mixing, a high incoming solar radiative flux absorbed in the first meters of the ocean can lead to the formation of a DWL (Price et al., 1986; Fairall et al., 1996; Soloviev and Lukas, 1997; Kawai and Wada, 2007). The favourable conditions for a DWL development are encountered during periods of reduced atmospheric convection activity which are particularly prevalent during Madden–Julian Oscillation (MJO) suppressed phases (e.g Bellenger and Duvel, 2009). Though the thickness of a DWL is only confined to several meters, the layer can horizontally extend over a thousand kilometers and persist for several days (Bellenger and Duvel, 2009; Matthews et al., 2014). Based on a 1979-2002 daily time series over the tropics, Bellenger and Duvel (2009) showed that DWL occur over large regions in both Indian and Pacific tropical basins, in particular prior to monsoon onset. Matthews et al. (2014) identified that a DWL occurs on 25% of days in the tropical warm pool region of the Indian Ocean and western Pacific, with a higher frequency during the MJO suppressed phases. The equatorial Indian Ocean particularly is a hot spot of strong DWL development. The presence of DWL is assumed to play an important role in intraseasonal tropical oscillation (i.e. MJO) in the equatorial Indian Ocean (Woolnough et al., 2000; Bellenger and Duvel, 2009; Moum et al., 2014; Jiang et al., 2020).

The high amplitudes of the SST diurnal variability associated to a DWL have a significant impact on the thermodynamic and turbulence structure of the marine atmospheric boundary layer (MABL). In response to a DWL, which drives a daytime increase of turbulent surface heat and moisture fluxes, the MABL deepens (Johnson et al., 2001; Johnson and Ciesielski, 2017) and the diurnally modulated turbulent field can exhibit particular organizations in open cells or horizontal convective rolls (Ruppert and Johnson, 2015). The atmospheric convection can thus be broadly modified. In the absence of a DWL, the typical daytime evolution of the atmospheric convection exhibits a peak in the early morning (Yang and Slingo, 2001; Bowman et al., 2005) with a weak diurnal variability. In contrast, when a DWL is established, the convection is more analogous to continental signals with an increase around noon and a maximum in the afternoon (Khairoutdinov and Randall, 2006; Bellenger et al., 2010; Ruppert and Johnson, 2015, 2016). These processes participate in the build-up of moisture during the MJO preconditioning phase, a key feature for the MJO onset (Seo et al., 2014; Ruppert and Johnson, 2016; Jiang et al., 2020).

Besides the large occurrence of DWL, the detailed understanding of the local energetic processes down to diurnal time scales remains an open question especially as they affect the whole Ocean-Atmosphere coupled system up to the climate scale (Ham et al., 2010; Terray et al., 2012; Masson et al., 2012). Whatever the resolution of the considered model from the global to the local scale, the proper representation of MABL processes is fundamental since they control the mass and energy exchanges between the surface and the free atmosphere (Teixeira et al., 2008). This is especially prevalent in the presence of a DWL, given the non-linear interplays of the mechanisms involved. The lack of representation of those local processes impacts averaged fluxes and therefore potentially climate simulations (Bernie et al., 2008; Bellenger and Duvel, 2009; Matthews et al., 2014). Large and Caron (2015) used an empirical scheme to represent the sea surface diurnal cycle and revealed its impact on the atmosphere at a large scale. A better modeling of the diurnal cycle over the ocean has been also shown to have a clear positive effect on the intraseasonal to interannual variability (Flato et al., 2013). One of our objective is to disentangle the different processes at play in the evolution of a DWL and to present a reference case study to evaluate and improve their representation in coupled regional

and global models.

Nowadays, only few numerical studies focus on local-scale processes at play in ocean-atmosphere coupling systems. Developed reference cases for Large-eddy simulations (LES) have generally only focused on one of the components of the coupled system. In MABL studies with LES models, the air-sea interface is thus seen as a model boundary and not as an interactive zone. For example, in the First International Satellite Cloud Climatology Project (ISCCP) Regional Experiment (FIRE) case study dedicated to the marine stratocumulus diurnal cycle, the SST is kept fixed (Duynkerke et al., 2004). The same is true in the more recent Rain in Cumulus over the Ocean (RICO) case study investigating the evolution of trade–wind cumulus convection (vanZanten et al., 2011). The turbulent surface fluxes can also be fixed, as in the Barbados Oceanographic and Meteorological Experiment (BOMEX) case study investigating the marine shallow cumulus convection (Siebesma et al., 2003). More recently, case studies of cold air outbreak have been performed with a prescribed time-varying SST in order to represent the transport of a cold and dry air mass over a warmer sea (e.g., Roode et al. (2019) in the CONSTRAIN case, Brilouet et al. (2019) in a HyMeX case). A lagrangian approach has also been proposed by Sandu and Stevens (2011) or Lemarié et al. (2020), with an air mass advected over a changing SST, mimicking the presence of a SST front. Concerning the upper oceanic layer, most numerical studies focusing on the DWL mechanisms are based on one-dimensional oceanic models such as Shinoda (2005) and Karagali et al. (2017) exploring the role of the solar radiation, Giglio et al. (2017) focusing on the effect of wind gusts on diurnal variability and Reffray et al. (2015) studying the sensitivity to the turbulent vertical mixing. High-resolution simulations that explicitly resolve the relevant physical processes exist independently for the atmosphere and for the ocean. To our knowledge, no case studies exist using coupled ocean-atmosphere simulating systems. A framework with an atmospheric LES forced by an evolving SST deduced from a closed surface energy budget (a 1 m slab ocean model) has been recently proposed by Tan et al. (2016). They highlighted the opportunities given by allowing feedback between the MABL and the sea surface and emphasized that sensitivity to SST changes are not necessarily energetically consistent in previous studies of MABL clouds.

In the present work, we present the construction of a case study based on the Dynamics of the Madden–Julian Oscillation (DYNAMO) field observations, focusing on a DWL, with a 1-D oceanic mixed layer model using very high vertical resolution in the upper ocean. The novelty consists in using a coupled O-A framework with an atmospheric LES coupled to a 1-D oceanic model. With this case study, we have the objective to quantify the key processes involved in the establishment and decay of the DWL and the impact of coupling on the MABL. This represents a first step towards the underlying objective of designing a coupled framework based on LES for both the ocean and the atmosphere.

The paper is organized as follows: the observation data available to build and validate the case study and the coupled modelling strategy are presented in Section 2. Section 3 is devoted to the key processes involved in the DWL development and the ability of the 1-D oceanic model to realistically reproduce a DWL. Section 4 is dedicated to the validation of the coupled LES with the 1-D oceanic model through the comparison with observations. The last section concludes the paper with a discussion of the main results.

2 | CASE STUDY AND MODELLING STRATEGY

2.1 | Observations Available for the Case Study

The DYNAMO field campaign (Yoneyama et al., 2013) focused on the mechanisms governing the preconditioning of deep convection leading to a MJO active phase. This field campaign was conducted from boreal fall 2011 to early 2012 over the tropical Indian Ocean. Among all the instrumented sites, the research vessel (R/V) Revelle was deployed at the equator and 80.5°E, an area representative of open-ocean conditions and thus perfectly adapted for the present case study. This vessel was particularly well instrumented in order to document jointly the mean structure of the atmospheric and oceanic boundary layers

as well as the energy exchanges at the interface. Table 1 summarizes the observations used to build the present case study for the MJO suppressed phase monitored in November 2011 (see Moum et al. (2014) for a detailed description of the available data). Every three hours, radiosoundes were launched from the R/V Revelle in order to characterize the mean thermodynamic structure of the MABL. In addition, the high–resolution Doppler lidar and the ceilometer provided a continuous documentation of the wind and the cloud base, respectively. The air–sea interface was monitored with continuous measurements of SST and meteorological parameters (temperature, humidity and wind), downward radiative shortwave and longwave fluxes. For the period of interest with light wind conditions, estimates of air–sea turbulent fluxes using eddy–covariance or inertial–dissipation methods were not accurate enough due to sampling variability and motion corrections issues, particularly critical under these wind conditions (Marion, 2014). The turbulent fluxes have been thus estimated from the COARE3.0 bulk algorithm (Fairall et al., 2003). Bulk fluxes present some uncertainties, specifically under strong wind conditions (Brilouet et al., 2017) but also, as presently, in light wind conditions (Brunke et al., 2003). The upper layer of the ocean was monitored with two CTD profiles (Conductivity–Temperature–Depth) per day, combined with Chameleon data profiler (Moum, 1990) providing profiles of temperature, salinity and density every 20 minutes. The oceanic current velocity was measured hourly using an Acoustic Doppler Current Profiler (ADCP).

TABLE 1 Available observations at the R/V Revelle during the DYNAMO field campaign, covering the MJO suppressed phase of nov. 2011 and used either to build the simulated case study or for its validation.

	Type	Sample frequency	Resolution *	Data available	References
Atmospheric layer					
	Radiosoundings	8 per day	z_1 at 50–100 m $\Delta z \sim 5$ m	temperature humidity wind components	Earth Observing Laboratory (2014) Ciesielski et al. (2014)
	Doppler lidar	20 min	z_1 at 15 m $\Delta z \sim 5$ m	wind speed wind direction	Brewer (2013)
	Ceilometer	15 sec	–	cloud base	Johnson and Ciesielski (2017)
Air–sea interface					
	Meteorological station	10min	–	basic thermodynamic fields	Moum et al. (2014) de Szoeke et al. (2015)
	Turbulent fluxes **	10min	–	latent heat flux sensible heat flux wind stress	
	Radiometers	10 min	–	downward shortwave radiation downward longwave radiation	
Oceanic layer					
	CTD profiles	2 per day	d_1 at 1–2 m $\Delta d \sim 0.1$ m	temperature salinity density	de Szoeke et al. (2015)
	Chameleon Data	20 min	d_1 at 1–3 m $\Delta d \sim 1$ m	temperature salinity density	
	ADCP	1 hour	d_1 at 12–16 m $\Delta d \sim 10$ m	current velocity	

* The 'Resolution' column provides information about the height, z_1, (and respectively the depth d_1 for the ocean) of the closest point to the surface and an estimation of the vertical resolution.

** The turbulent fluxes have been computed using the COARE3.0 bulk algorithm (Fairall et al., 2003) with the mean meteorological observations at the R/V Revelle.

The time evolution of wind speed inside the MABL during November 2011 (Fig. 1a), emphasizes light–wind conditions encountered from 14 to 17 of November, a period of inhibited deep convection. The wind speed did not exceed 5 m s^{-1} inside the entire MABL during several days in a row. The low-level wind speed tends to increase during the afternoon as mentioned by Johnson and Ciesielski (2017) for DYNAMO and already observed by Johnson et al. (2001) during the Tropical Ocean and Global Atmosphere Coupled Ocean–Atmosphere Response Experiment field campaign (TOGA COARE). They related this increase to a more intense buoyancy–driven turbulence activity. After this light wind period, the wind experiences an abrupt change with a wind burst corresponding to the beginning of the MJO active phase on the 24 nov. 2011 (Moum et al., 2014). The SST time serie presented in Fig. 1b exhibits a strongly pronounced diurnal cycle during the MJO suppressed phase. The diurnal amplitude of the SST is on average around 1.5° C and reaches 2.8° C on 16 November over a time lapse of 9 h. Over the inactive MJO period, the daily-mean SST regularly increases. As noticed by Matthews et al. (2014), the presence of a DWL leads to a higher daily-mean SST due to the accumulation of energy in the upper–ocean layer. This process is crucial in the preconditioning of deep convection and the triggering of the MJO active phase (Woolnough et al., 2000; Bernie et al., 2005; Matthews et al., 2014). The downward shortwave radiative flux time serie (Fig. 1b) reflects the relatively clear sky conditions encountered above the R/V Revelle with a weak cloud attenuation. The 20 and 22 of November are notable examples where the cloud cover may have induced a weakening of the SST diurnal cycle. Under clear sky conditions, the SST peaks generally in the afternoon around 1600 LT. The downward shortwave radiative flux and the SST diurnal peaks are thus phase shifted of around 4 hours (Price et al., 1986; Shinoda, 2005; Kawai and Wada, 2007). The time serie of the surface wind speed, also sketched in Fig. 1b, confirms the light wind conditions during this suppressed period and the increases of the surface wind speed during the afternoons. As soon as the MJO phase gets active, the surface signals are unambiguous, the wind burst reaches up to 16 m s^{-1} and the SST collapses. The atmospheric conditions encountered during this MJO suppressed phase, i.e. a high solar forcing combined with low wind speed, are favourable for the development of DWLs. The upper–ocean temperature structure, presented in Fig. 1c, is indeed stably stratified during daytime due to the accumulation of solar energy.

Over the entire suppressed phase, we selected a 54-hour period, from the 13 nov. 2011 at 2300 LT to the 16 nov. 2011 at 0500 LT (the black frame in Fig. 1). During this period, from the surface up to the top of the MABL, light wind conditions are persistent and the MABL does not present any wind shear. The downward shortwave radiation is only slightly affected by the cloud cover and almost clear sky conditions can be considered. With respect to both SST and ocean temperature observations, the diurnal response of the ocean to atmospheric forcing is significant over the two selected days with a particularly strong diurnal variability. A maximum of the SST amplitude is observed on the 16 nov. 2011, however the oceanic mixed layer does not exhibit a diurnal warm layer but rather a cooling of the water column that can be induced by horizontal advection and/or cold water lenses. These processes are, at this time, too complex to be correctly taken into account in the present modeling approach. In order to validate the novel numerical strategy presented here, an atmospheric LES coupled with an 1-D oceanic model on each surface grid point, the 54h selected period provides an ideal framework for the build–up of the present modelling case study to investigate over two consecutive days the establishment, development and dissipation of a DWL as well as its impact on the diurnal variability of the MABL mean and turbulent structures.

2.2 | Modelling Framework of the ocean-atmosphere coupled system

2.2.1 | Modelling Strategy

The two main objectives of this study are: 1/ to assess whether a 1-D oceanic model is able to reproduce the observed time evolution of DWL and how radiation absorption, turbulence and atmospheric forcing affect its characteristics and 2/ to build a case to analyze the DWL impact on the atmosphere. To this aim, we carried out numerical simulations of the case study presented

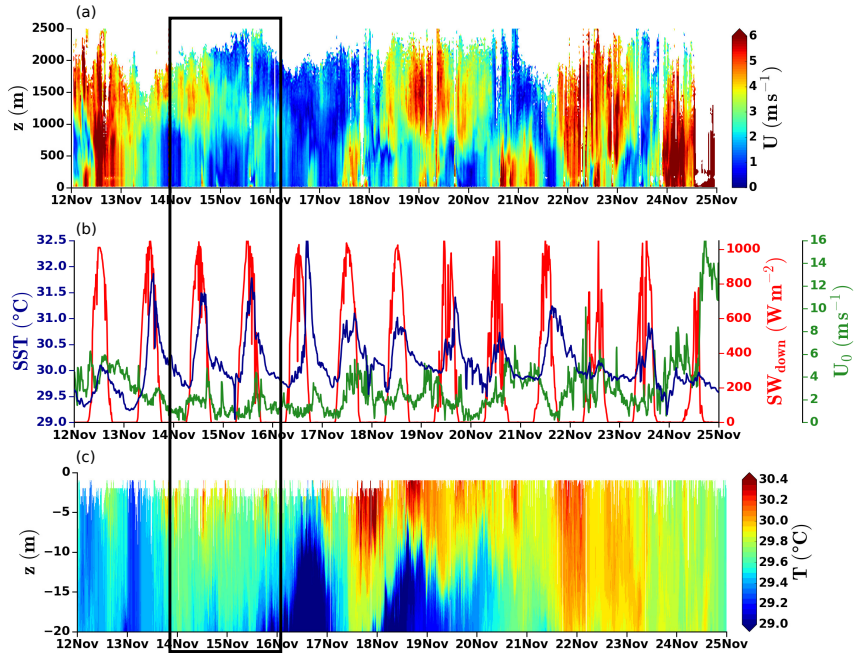

FIGURE 1 (a) Time-height cross-section of wind speed (U) measured from a high-resolution Doppler Lidar inside the MABL, (b) time series of sea surface temperature (SST) from the SeaSnake, downward shortwave radiation (SW_{down}) from a radiometer and wind speed close to the surface (U_0) from a meteorological station and (c) time-depth cross-section of temperature (T) in the ocean monitored with the Chameleon profiler. The data were monitored at R/V Revelle during the leg 3 of the DYNAMO field campaign. The black square refers to the 54 h interval selected for the simulation.

above. For the first objective we used a 1-D ocean model forced with atmospheric fields. Once this reference simulation has been evaluated with the available observations, we performed a suite of sensitivity tests in order to highlight the main processes involved in the DWL growth and collapse. For the second objective, we used a 3D atmospheric LES model coupled at each of its surface grid point with a 1-D oceanic model. The results of these two ocean experiments (forced and coupled) enable to assess the impact of atmospheric forcing on a DWL and to analyze the response of the MABL to the coupling.

2.2.2 | The One–dimensional Oceanic Model and the Oceanic Set–up

The 1-D oceanic model is used first to check its capability of reproducing the DWL, then in coupled mode with the Meso-NH atmospheric model (Lac et al., 2018). Whatever the configuration the SST is explicitly solved by the oceanic model. The ocean model used is the one-dimensional model of Gaspar et al. (1990) with a prognostic equation of the turbulent kinetic energy (TKE) with a 1.5-order closure, inserted in the surface module SURFEX of the Meso-NH model (Lebeaupin Brossier et al., 2009). The other prognostic variables are the ocean temperature, salinity and horizontal current components. Based on sensitivity tests to ensure the convergence of results (not shown here), the simulations are performed with a time step of 5 sec. The z-vertical grid has been chosen to be able to reproduce the thin DWL: a constant 10 cm grid mesh from the surface down to 5 m depth, then a progressively stretched grid mesh from 5 m to 20 m down to 50 m depth, then a constant grid mesh of 50 m. Since the observed

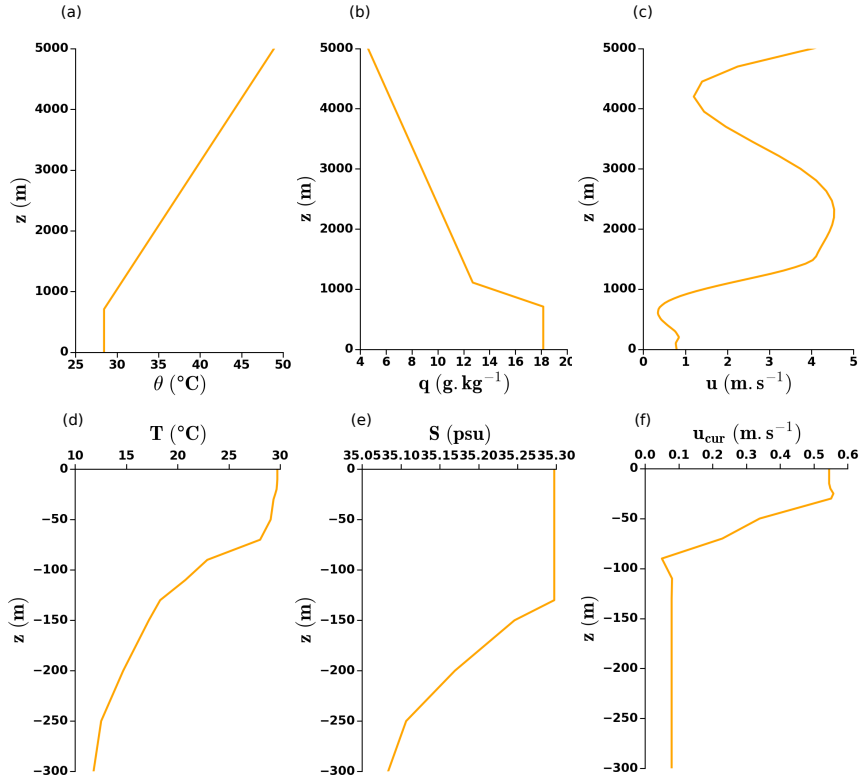

FIGURE 2 Profiles of (a) potential temperature (θ), (b) specific humidity (q) and (c) zonal wind speed (u) used to initialize the atmospheric part of the simulation. The profiles are obtained from a smoothing of the the sounding performed the 13 nov. 2011 at 2351 LT on the R/V Revelle. Profiles of (d) temperature, (e) salinity and (f) current used to initialize the 1-D ocean model. The profiles are obtained from a smoothing of the CTD sounding performed the 13 nov. 2011 around 22 LT. ADCP data are used and extrapolated up to the surface for the oceanic current.

oceanic temperature at 10 m depth is steady for these two days (Fig. 1c), neglecting the large scale horizontal advection is a reasonable assumption and no large-scale tendency of temperature is prescribed. The initial state of the ocean, derived from observations, is presented in Figure 2d, e, f. A slightly stable layer is apparent on the temperature down to 80 m while the salinity is well mixed down to 140 m. The oceanic current is relaxed toward the initial profile with a relaxation timescale of 24 h enabling diurnal variations.

The surface heat budget is the sum of the shortwave (solar) flux (SW_{net}), the longwave (infrared) flux (LW_{net}), and the sensible and the latent heat fluxes. The downward SW (SW_{down}) forcing comes from the R/V Revelle observations (Fig. 1b) and a small fraction of it, the upward SW (SW_{up}) is reflected, depending on the albedo and calculated in the oceanic model. The net shortwave flux is strongly positive, a large part of SW_{down} radiative flux penetrates in the ocean. This SW_{net} radiation is absorbed in the ocean column, providing a heat source (Soloviev and Lukas, 2014). The longwave radiation emitted from the sea surface (LW_{up}) is computed using the ocean model SST with the assumption that the ocean radiates as a gray body and therefore LW_{up} is proportional to $(SST)^4$. The turbulent heat fluxes H and LE (and the wind stress $\vec{\tau}$) are computed with the iterative bulk parameterization COARE3.0 (Fairall et al., 2003) using the prognostic SST provided by the 1-D oceanic model and the atmospheric variables observed by the R/V Revelle such as the temperature, the moisture and the relative wind taking into

account the surface current. The non-solar heating term at the surface F_{nsol} is then the sum of sensible, latent and net LW_{net} fluxes:

$$F_{nsol} = H + LE + LW_{net} \tag{1}$$

The last forcing field required by the oceanic model is the precipitation rate, which is given by the R/V Revelle observations.

The one-dimensional equation of temperature can be expressed as:

$$\underbrace{\frac{\partial T}{\partial t}}_{TEND} = \underbrace{\frac{SW_{net}}{\rho_0 c_p}\frac{\partial I(z)}{\partial z}}_{DTFSOL} \underbrace{- \frac{\partial \overline{w'T'}}{\partial z}}_{TURB}, \tag{2}$$

where the temperature tendency (TEND) is decomposed into a source of energy from the penetrating SW radiations (DTFSOL) and a term of vertical mixing (TURB).

The boundary condition for $TURB$ is given by

$$-\overline{w'T'}(z=0) = \frac{F_{nsol}}{\rho_0 c_p}, \tag{3}$$

where ρ_0 and c_p are the reference density and specific heat at a constant pressure of seawater, respectively. $I(z)$ is the vertical absorption of the shortwave radiative heat flux. The penetration of the SW radiation depends on numerous factors as the sun angle, the cloud cover or the water colour depending on chlorophyll concentration (Ohlmann et al., 2000). Following Paulson and Simpson (1977), $I(z)$ is expressed as a sum of exponential terms:

$$I(z) = A_1 e^{-z/\lambda_1} + (1 - A_1) e^{-z/\lambda_2}, \tag{4}$$

where z is the depth (positive downward) and A_1 an attenuation parameter. The two length scales, λ_1 and λ_2, are penetration depths corresponding to absorption by the red and blue-green parts of the solar spectrum, respectively. As this vertical absorption $I(z)$ is a key process in term of energy distribution inside the ocean layer, we carried out sensitivity tests on its expression and vertical discretization as detailed in Sect. 3.2.1.

2.2.3 | The Meso-NH Model and the Atmospheric Set–up

The MABL evolution is simulated with Meso-NH (Lac et al., 2018), a non-hydrostatic atmospheric research model sharing its physics with the French operational model AROME (Seity et al., 2011). In the present LES runs, the momentum components are advected with a fourth-order centered scheme whereas the scalar variables are advected with a piece-wise parabolic method scheme from Colella and Woodward (1984). A fourth-order explicit Runge–Kutta method is applied for the timestepping. Concerning the physical parameterizations, mixed-phase clouds are handled by a warm microphysical scheme (Kessler, 1969) which allows transformations between vapor, cloud water and rain water. The radiative transfers are computed based on the ECMWF operational radiative code (Gregory et al., 2000). The turbulence scheme (Cuxart et al., 2000) is based on a 1.5-order closure with a prognostic equation of the TKE derived from Redelsperger and Sommeria (1986). The mixing length is defined as the cubic root of the three mesh sides, with a correction depending on stratification (Deardorff, 1980).

For the LES, we chose an horizontal domain of 30 km × 30 km that is large enough to capture the mesoscale organization of the turbulent field into horizontal convective rolls or open cells (Weckwerth et al., 1996; de Roode et al., 2004). The simulation can be defined as an LES if at least $70 - 80\%$ of the TKE is explicitly resolved (Pope, 2000). It is recognized that about ten grid points are needed to correctly reproduce a turbulent structure and the thermodynamic horizontal characteristic length scale are in the order of magnitude of the MABL depth (de Roode et al., 2004). During the suppressed periods of the DYNAMO field campaign, Johnson and Ciesielski (2017) observed MABL depths of around 600 m at the R/V Revelle. The LES is thus performed with a horizontal resolution of 50 m. The vertical grid is composed of 78 levels with a resolution of 10 m close to the surface, progressively stretched to 250 m above 3 km up to the top of the model at 5 km. With this stretched grid, there are around 35 vertical levels inside the MABL with a resolution of 30 m at its top (i.e. around 600 m). Periodic lateral boundary conditions are applied and an absorbing layer is added at the top of the domain to prevent the reflection of gravity waves. The simulation starts the 13 nov. 2011 at 2300 LT for a duration of 54 hours.

The atmospheric model is initialized with horizontally homogeneous profiles of potential temperature, specific humidity and wind component presented in Fig. 2a,b,c. Those profiles, derived from the R/V Revelle radiosounding the 13 nov. 2011 at 2351 LT, have been smoothed in order to remove the small scale vertical variability which cannot be captured by the model. As the LES configuration is a limited-area domain, the large-scale conditions must be prescribed. Close to the equator, the Coriolis effect becomes negligible and the horizontal temperature gradients are known to be small in the Tropics (Sobel et al., 2001). Due to the light wind conditions, the large-scale horizontal advection of temperature and humidity are assumed to be negligible compared to the other budget terms whereas a large-scale vertical velocity w_{LS} has to be prescribed (Sobel et al., 2014; Ruppert and Johnson, 2015). The determination of w_{LS} remains one of the greatest long-standing observational challenges of atmospheric science, especially for fair weather tropical condition (see Bony and Stevens (2019) for a review and discussion). Whereas its magnitude is small compared to the horizontal wind, w_{LS} largely controls the vertical distribution of atmospheric water vapour. The last 25 years of tropical boundary layer research based on idealized simulations of the atmosphere with SCM, CRM or LES, have pointed out that w_{LS} is a critical forcing unconstrained by observations (e.g. Sobel and Bretherton (2000)). In this study, the large–scale vertical velocity has been estimated, at the first order, following a radiative–convective equilibrium (Sobel and Bretherton, 2000; Mapes, 2001). Details about the method are presented in appendix A. The prescribed large—scale vertical velocity is then chosen to be constant in time and equals the time average over 54 hours, corresponding to the duration of the simulation. As the characteristic timescales of large-scale conditions are much larger than those of the boundary layer processes studied here, this assumption appears reasonable. As the case study is localized in the tropical region where the dynamics is complex (linked for example to the influence of the waves, the temporal and spatial variability or the light wind conditions), the model, with a closed-area domain, is not able to reproduce the mesoscale dynamics complexity. To cope with this, a 3-hour nudging of the mean wind (i.e. horizontally averaged wind in LES case) is applied towards the observed R/V Revelle wind profiles. Varying this time scale in LES shows weak sensitivity.

In this configuration, the atmospheric model is coupled at each grid point of the surface domain, to an oceanic column. The oceanic columns are independent of each other, no information is exchanged horizontally between the oceanic columns.All the forcing fields transmitted to the oceanic model are computed by Meso-NH in its surface scheme. The forcing fields are composed of the net radiative fluxes SW_{net} (solar) and LW_{net} (infrared), the turbulent fluxes (latent heat, sensible heat and momentum) using the COARE3.0 algorithm (Fairall et al., 2003) as in the forced configuration, and the simulated precipitation rate. These parameters are then transmitted at each surface grid point to the different and independent oceanic columns. Each 1-D ocean model computes the prognostic evolution of temperature, salinity, horizontal current components and turbulent kinetic energy profiles. Then, the SST value estimated by each oceanic column with the 1-D model is transmitted to the atmospheric model for the next time step calculations, in particular for computing LW up and the surface turbulent heat fluxes. Simulated horizontal surface currents are not used for flux computation nor in the atmospheric model for turbulence to avoid spurious dynamical discontinuities to propagate in the MABL.

3 | REPRODUCING A DIURNAL WARM LAYER WITH A 1-D OCEANIC MODEL

3.1 | Reference Configuration

The results presented in this section are obtained with the reference 1-D ocean experiment, forced by the 10-min R/V Revelle atmospheric observations. This permits to investigate the representation of the DWL formation and life-cycle in the model with a controlled atmospheric forcing. The SST and surface turbulent fluxes are computed by the 1-D oceanic model.

3.1.1 | Surface time evolution

In this reference simulation, the diurnal variation of SST (Fig. 3a) is reproduced with a good temporal correlation and primarily linked with the SW_{down} time evolution (Fig. 3c). The peak is reached in the afternoon between 1600 LT and 1700 LT as found by Matthews et al. (2014) or Large and Caron (2015). The amplitude of the observed and simulated daily SST variations are very close with $\Delta SST_{obs} = 1.83\,°C$ and $\Delta SST_{simu} = 1.79\,°C$ for the first day. Differences on the second day are higher with $\Delta SST_{obs} = 2.15\,°C$ and $\Delta SST_{simu} = 2.40\,°C$. The increase of daily-averaged SST between the two days is 0.29°C and 0.06°C for the simulation and the observations, respectively. This slight discrepancy can come from large scale temperature advection neglected in the simulation as not measured during the field experiment. Once the SST peak is reached in the afternoon and the SW flux decreases, the decrease of SST is however faster in observations than in models. This rapid SST decay is probably due to the surface wind speed peak observed at 1600 LT (Fig. 3a). This induces corresponding peaks in the turbulent heat fluxes (Fig. 3b). As suggested by Bellenger et al. (2010), the increase of surface wind can be partly linked with the convective gusts. The observed nocturnal state (after 2300 LT) is correctly reproduced by the model.

As seen above, the non-solar surface heat flux (Eq. 1) is largely controlled by the SST. The variations of LW_{up} and the discrepancies between simulation and observations (Fig. 3e) reproduce those of the SST. The surface latent and sensible heat flux (Fig. 3b) are modulated by the SST and the wind speed. They show a diurnal evolution of around 150 W m^{-2} and 20 W m^{-2}, respectively, which is influenced by the SST diurnal evolution, and the discrepancies between simulation and observations are correlated with the SST difference described above. Their evolution is also strongly correlated with that of the surface wind speed (Fig. 3a) as previously observed by Ruppert and Johnson (2015, 2016). The resulting non-solar heat flux is typically of the order of 100 W m^{-2} with peaks up to 300 W m^{-2}, consistent with suppressed conditions in tropical regions. The larger differences between observations and simulation are due to SST differences, and the time evolution is largely controlled by the wind speed. The SST exerts a clear negative feedback on the atmosphere through the longwave upward radiative flux and turbulent (mainly latent) heat fluxes.

The downward shortwave radiation forcing, presented in Fig. 3c, follows almost a clear sky temporal evolution, with only small shallow cumuli passing over the R/V Revelle sampling area for the first day, except for the second day around 1600 LT with a sharp fall, probably associated with few cumuli. The small differences between the upward shortwave radiations observed and simulated are linked to the albedo. The observed SW_{up} has been determined with a fixed albedo of 5.5% whereas the simulated albedo depends on several parameters (such as the solar zenithal angle). Finally, the upward and downward longwave radiative fluxes (Fig. 3d) present small variations reflecting nearly clear sky conditions. During the day, these variations are consistent with the solar radiations, which confirm the passage of few clouds.

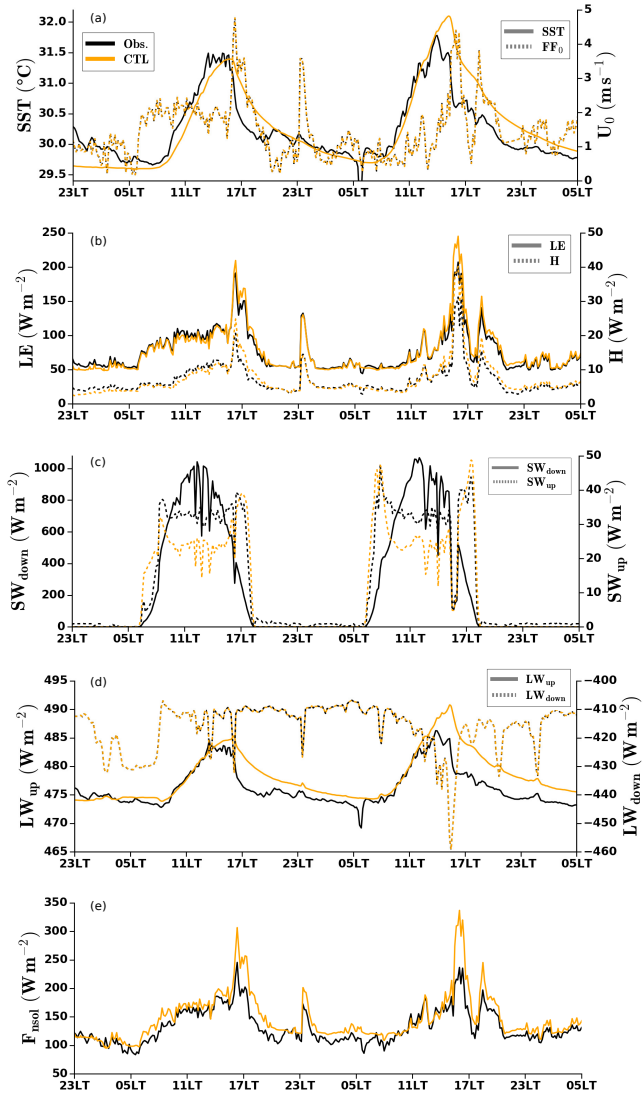

FIGURE 3 Time series of (a) the sea surface temperature (solid lines) and surface wind speed (dashed lines), (b) latent heat flux (solid lines) and sensible heat flux (dashed lines), (c) downward shortwave radiation (solid line) and upward shortwave radiation (dashed lines), (d) upward longwave radiation (solid lines) and downward longwave radiation (dashed lines) and (e) non-solar heating $F_{nsol} = LW_{up} - LW_{down} + LE + H$. The black lines are the observations from the R/V Revelle and the orange lines (CTL) correspond to the reference oceanic simulation. The fluxes are counted positive when they correspond to a gain of energy for the atmosphere (i.e. a loss of energy for the ocean).

3.1.2 | Time evolution of the oceanic mixed layer

The time–depth cross–section of the oceanic temperature is presented in Fig. 4a. The initial well-mixed isothermal profile of the oceanic mixed layer is progressively cooled during the night, reaching a temperature minimum of $29.65\,°C$ at 0600 LT. After

sunrise, the upper layer of the ocean absorbing the SW radiation is warmed with a temperature variation at 1 m depth reaching $1.30\,°C$ from 0600 LT to 1600LT for the first day and $1.38\,°C$ for the second one. In order to characterize the simulated DWL in terms of depth and temporal extent, the analysis developed by Matthews et al. (2014) has been applied. The DWL depth is defined here as the depth of a fixed isotherm (T_*) linked to the minimum temperature (T_{min}) at d=0.5 m and the maximum value over a period of 24 h (T_{max}) as follows:

$$d_{DWL} = d(T = T_*), \tag{5}$$

with

$$T_* = T_{min} + \alpha\,(T_{max} - T_{min})\,, \tag{6}$$

and α fixed at 0.3 (Matthews et al., 2014). The temporal extent of the DWL is then defined as the duration over which its thickness is not null (thick black contour in Fig. 4). The DWL is thicker on the first day than on the second one with maximum depths of 2.9 m and 2.3 m, and duration of 15h 17 mn and 14h 40 mn, respectively. However, the diurnal variation magnitude in the first meter is higher for the second day because the solar energy is trapped over a thinner layer. As already observed by Moulin et al. (2018), in light wind conditions the wind-driven mixing is too weak to destabilize the confined near-surface layer. Here, wind conditions over the 0500LT – 1700LT time interval are lighter on the second day with $\overline{U_0} = 1.29$ m s^{-1} compared to $\overline{U_0} = 2.05$ m s^{-1} on the first day, and they lead to a thinner but warmer DWL. Once the shortwave radiative flux decreases in the afternoon (Fig. 3c), the ocean loses energy due to surface heat exchanges and turbulent mixing of the upper layer (see below). It returns to isothermal conditions at the end of the night, just before sunrise.

The simulated DWL are now compared with observations. Because DWL is shallow, its proper sampling requires a very fine vertical resolution close to the surface. Unfortunately, for the current period of interest, the available observations were too coarse to properly describe the upper–ocean structure in the first meters below the surface. Also, the instruments need time to stabilize themselves in the water, CTD and Chameleon do not provide measurements in the first two meters. The junction of the observed temperature profiles with the SST measured on the R/V Revelle must be considered with prudence. Therefore, the comparison of the observations and the simulated fields in this subsurface region should be taken with caution. Comparisons between simulated and observed profiles of temperature for the two days are presented in Fig. 4f and Fig. 4g. Despite a slightly colder behaviour in the simulation the first day, the simulated and observed temperature profiles are in agreement below 2 m depth. As discussed in the previous section, the SST (black and orange triangles) are very close to each other at 1300 LT. At 2200 LT (dashed lines in Fig. 4f and 4g), the differences between the simulated and observed DWLs are more pronounced. The observed temperature profiles present well-mixed behaviour which seems realistically extrapolated up to the surface whereas a warm layer signal remains in the simulated temperature profiles. We interpret this delay in the collapse of the DWL as due to the vertical mixing, which is probably not sufficiently efficient here, under stably stratified conditions, to propagate downwards the SW heating close to the surface (Matthews et al., 2014).

The simulated oceanic current also exhibits a well marked diurnal evolution with a 2-h delay with respect to the DWL (Fig.4e). Large and Caron (2015) also noticed a surface current reaching its peak in the afternoon, delayed with the temperature maximum. Its peak value of 0.17 m s^{-1} agrees with observational studies, such as Sutherland et al. (2016) who observed a diurnal jet of 0.15 m s^{-1} or Kudryavtsev and Soloviev (1990) with a current anomaly up to 0.19 m s^{-1}. Due to the stably stratified structures of the DWL, the wind-driven momentum is trapped and leads to a diurnal jet (Price et al., 1986; Cronin and Kessler, 2009; Smyth et al., 2013).

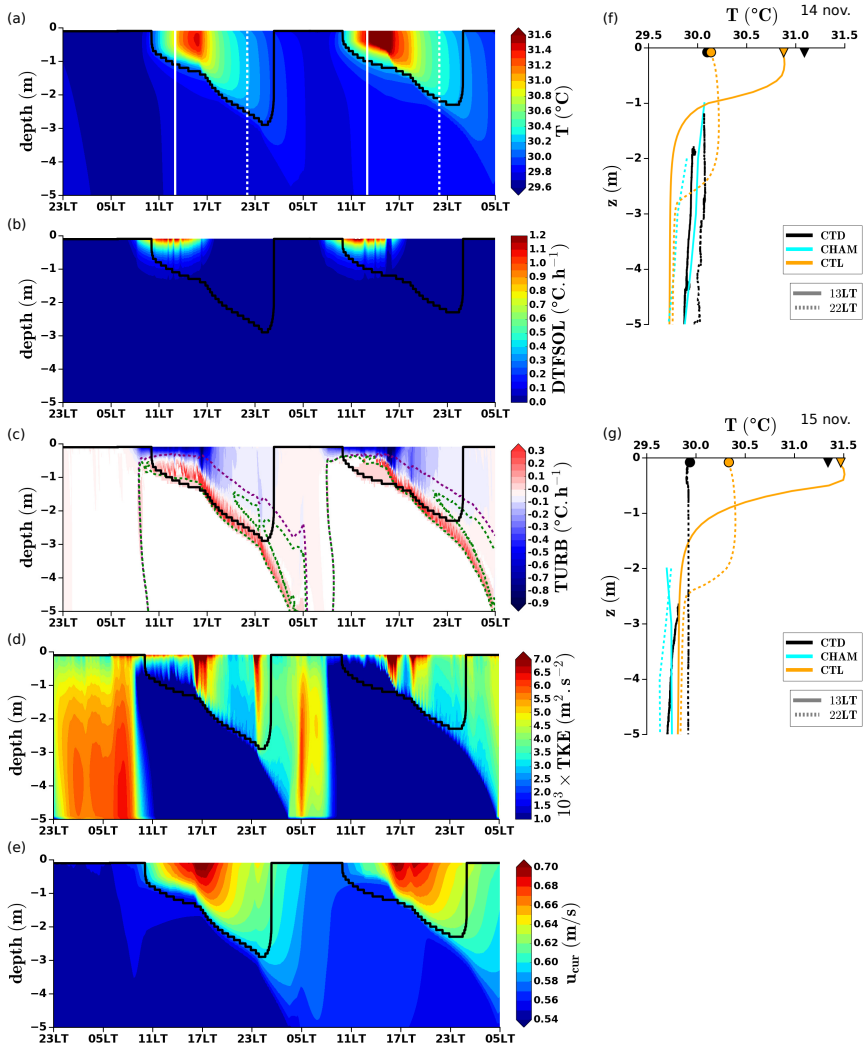

FIGURE 4 Time-depth cross-section of (a) the temperature (T) inside the oceanic mixed layer, (b) the absorbed SW radiation (DTFSOL) and (c) the vertical turbulent mixing (TURB) as the terms of the heat budget (eq. 2), (d) the turbulent kinetic energy (TKE) and (e) the current (u_{cur}). The thick black contour represents the depth of the DWL, the purple and green dashed-lines in (c) refer to $Ri = 0$ and $Ri = 1/4$, respectively. Simulated profiles of temperature (orange lines) compared to CTD profiles (black lines) and Chameleon data (cyan lines) (f) on the 14 nov. and (g) on the 15 nov., the solid and dashed lines correspond to 1300 LT and 2200 LT, respectively.

3.1.3 | Heat Budget in the Oceanic Mixed Layer

To quantify the role of the different processes controlling the DWL evolution, we explore here the evolution of the right-hand side terms of Eq. 2, namely the penetration of the SW radiations (DFTSOL) and the turbulent mixing (TURB) (Fig. 4b and c). The SW absorbed radiation is a predominant heat source over a very thin layer only, due to its exponential decay with depth. It reaches a maximum of 1.24 °C h^{-1} at the first oceanic model level (10 cm depth) but abruptly drops to 0.11 °C h^{-1} around 1 m.

TABLE 2 Summary of the three sets of sensitivity tests performed on the key processes driving the heat budget of the oceanic mixed layer: the solar heating (DTFSOL in Eq. 2), through the absorption of solar radiation with depth (eq. 4) and the effect of using different discretization methods, the wind-driven mixing through the wind stress and the heat loss through the surface air-sea exchanges (eq. 3).

		Solar coefficients			Penetrating profile	τ (N m^{-2})	U_0 (m s^{-1})	F_{nsol} (W m^{-2})
		A_1	λ_1 (m)	λ_2 (m)	discretization			
Reference	CTL	0.58	0.35	23	Compact exponential scheme	Bulk from atm. obs.	R/V Revelle obs.	R/V Revelle obs.
Solar	S1	0.58	0.35	23	1st-order finite differences	X	X	X
	S2	0.69	1.1	23	Compact exponential scheme	X	X	X
Dynamic	D1	X	X	X	X	Fixed to 0 N m^{-2}	X	X
	D2	X	X	X	X	$1.5 \times \tau_{CTL}$	X	X
Surface	SURF1	X	X	X	X	X	Fixed to 1.7 m s^{-1}	X
	SURF2	X	X	X	X	X	X	Fixed to 146 W m^{-2}

The DWL extension down to several meters is then controlled by other processes propagating this solar heating downwards.

In the following, we use the Richardson number (Fig. 4c) and the TKE evolution (Fig. 4d) to investigate the respective parts of buoyancy and dynamical mechanism (or shear instability) in the turbulent mixing. The Richarsdon is defined as $Ri = N^2/S^2$ with N^2 the buoyancy frequency and S^2, the shear magnitude. Three regions of the oceanic upper layer can be defined according to its values (Fig. 4c). The areas where $Ri < 0$ correspond to unstable thermal conditions (brown dashed-line for $Ri = 0$). Ri between 0 and $1/4$ characterize unstable dynamical conditions (between the purple dashed-line and the green dashed-line). The area where $Ri > 1/4$ characterizes stable conditions.

The time-depth evolution of Ri shows that, shortly after sunrise, the oceanic upper layer is thermally stable. Only a thin layer close to the surface remains thermally unstable, with strong TKE values. Caldwell et al. (1997) and Moulin et al. (2018) also observed a turbulence decay by an order of magnitude. During the day, the stability and the TKE in the oceanic upper layer increase, in link with the increase of the buoyancy frequency N^2 (not shown). When the DWL develops, the area of dynamic instability ($Ri \in [0, 1/4]$) increases and follows the bottom of the DWL. Turbulent mixing is thus generated through dynamical instabilities and erodes the DWL from below (Smyth et al., 2013; Moulin et al., 2018). The layer below is characterized by stable conditions ($Ri > 1/4$) and minimum values of TKE. At night, under low wind conditions, the main source of TKE is the buoyancy production. Before sunrise, the thermal instability extends to concern the whole layer, where the turbulence is also active.

The full cycle of DWL from its formation to its decay is thus controlled by the combination of several processes: absorbed solar radiation, surface heat loss and turbulent vertical mixing. The present simulation shows that the 1-D oceanic model is able to satisfactorily reproduce the evolution of these processes.

3.2 | Sensitivity tests

In order to isolate and better understand the role of these processes, three sets of sensitivity tests have been performed, focusing on the role of solar heating, turbulent mixing and surface cooling (Table 2). The role of DTFSOL is analyzed by varying the penetration profile. The dynamics is investigated by varying the wind stress and its contribution to the mechanical production of TKE. Finally, the surface cooling, the boundary condition of the ocean (Eq. 3) is considered.

3.2.1 | Absorption of the solar radiation

Though a key parameter for the DWL evolution, the solar radiation absorption profile is poorly constrained. Indeed, it is very difficult to measure because it concerns mostly the first meters of the ocean (Soloviev, 1982; Soloviev and Lukas, 1997; Shinoda, 2005). For instance, almost 50% of the solar energy is confined in the first 1.5 m at the R/V Revelle location during the DYNAMO field campaign (Moum et al., 2014; Matthews et al., 2014). Previous studies highlighted the impact of variations in chlorophyll concentrations, albedo or turbidity on the penetration profile (Ohlmann et al., 2000; Shinoda, 2005; Matthews et al., 2014). Here, we test the sensitivity to two combinations of absorption parameters involved in the formulation of $I(z)$ (eq. 4). Due to an exponential form of the penetration profile, it is very sensitive to the numerical computation of its vertical divergence (test S2, parameters A_1 and λ_1, λ_2 in Eq. 4). We also test the influence of the discretization method (S1). Figure 5 presents the differences of volume heat source and of temperature inside the oceanic layer compared to the control simulation. In the analysis, the focus is on the growth phase of the DWL since the solar absorption is expected to have the strongest impact on this period.

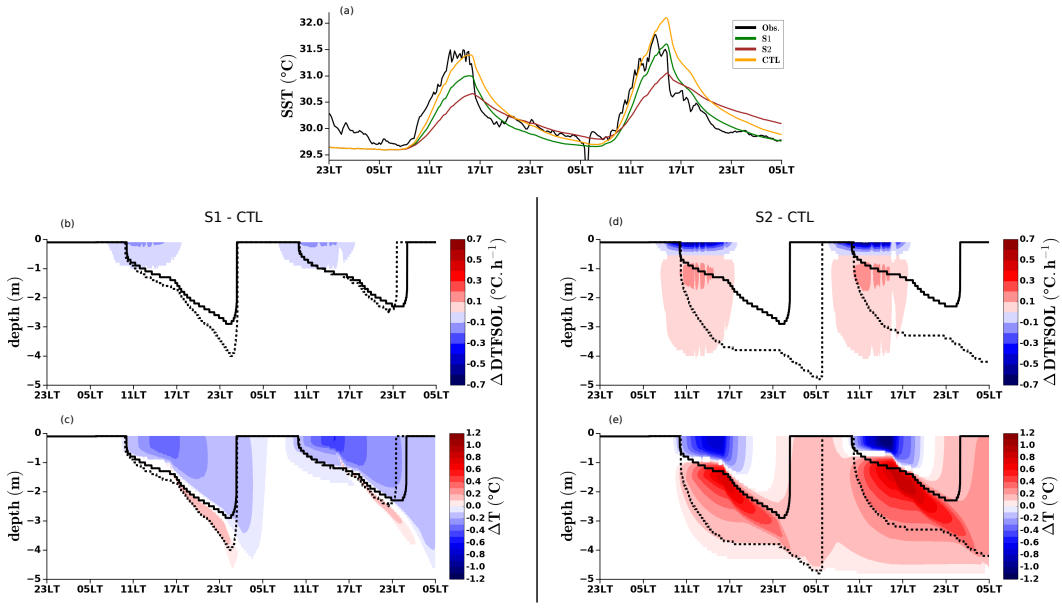

FIGURE 5 (a) Time series of the sea surface temperature (SST), the back line corresponds to the SST monitored at the R/V Revelle with a sea snake and the coloured lines correspond to the sensitivity tests listed in Table 2. Time–depth cross–sections of the difference the volume heat source induced by the absorption of solar radiation (the first term of the right hand side in eq. 2) and temperature between the simulations listed in Table 2 and the reference simulation (CTL). (b), (c) S1 and (d), (e) S2. The thick black contours represent the depth of the DWL for the reference (solid lines) and the test (dashed lines), respectively.

The way the profile is discretized (S1) directly impacts the volume concerned by the absorption of solar radiation as shown in Fig. 5b. A one-order finite difference method (coarse discretization) leads to a heat deficit close to the surface, part of the absorbed solar radiation is not being taken into account. An exponential profile (Compact Exponential Difference Scheme) ensures that no absorbed solar flux is , independently of the chosen mesh size. This is the discretization method used in the oceanic model NEMO, (standing for Nucleus for European Modelling of the Ocean) which is a modelling framework for research activities and forecasting services in ocean and climate sciences (Gurvan et al., 2019). The temperature differences at d=0.5 m can reach 0.48 °C and the formed DWL, whilst similar in thickness, is colder (cf. Fig. 5c). The SST amplitude is thus weaker and

the temporal correlation with the observations during the growing phase is also impaired. Changing the absorption coefficients (S2) also changes the energy distribution with a larger and deeper heat dilution (Fig. 5d), resulting in a thicker DWL (Fig. 5e). The agreement of the simulated SST with observations is lower, both for the DWL growth timing and its magnitude.

3.2.2 | Surface wind stress

The turbulent mixing propagates downwards the energy brought by solar heating. Near the surface, this mixing is controlled by the wind stress, even in the light-wind conditions corresponding to strong DWLs (Smyth et al., 2013; Giglio et al., 2017). We test here (Fig. 6) the effect of setting the wind stress to 0 (D1) or increasing it by 50% (D2).

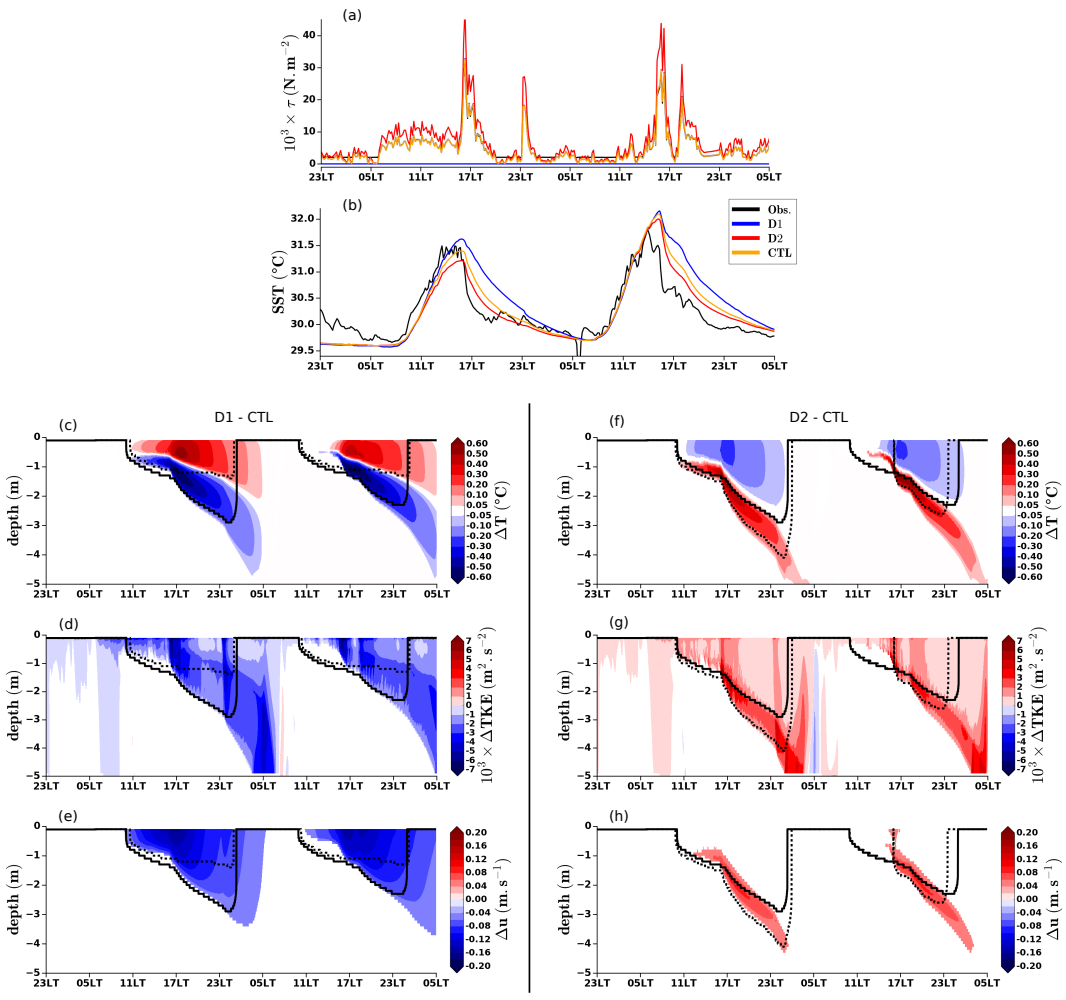

FIGURE 6 (a) Time series of the wind stress, (b) of the SST, time-depth cross-sections of the difference of temperature, TKE and current between the simulations listed in Table 2 and the reference simulation (CTL). (c), (d), (e) D1; (f), (g), (h) D2. The thick black contours represent the depth of the DWL for the reference (solid lines) and the test (dashed lines), respectively.

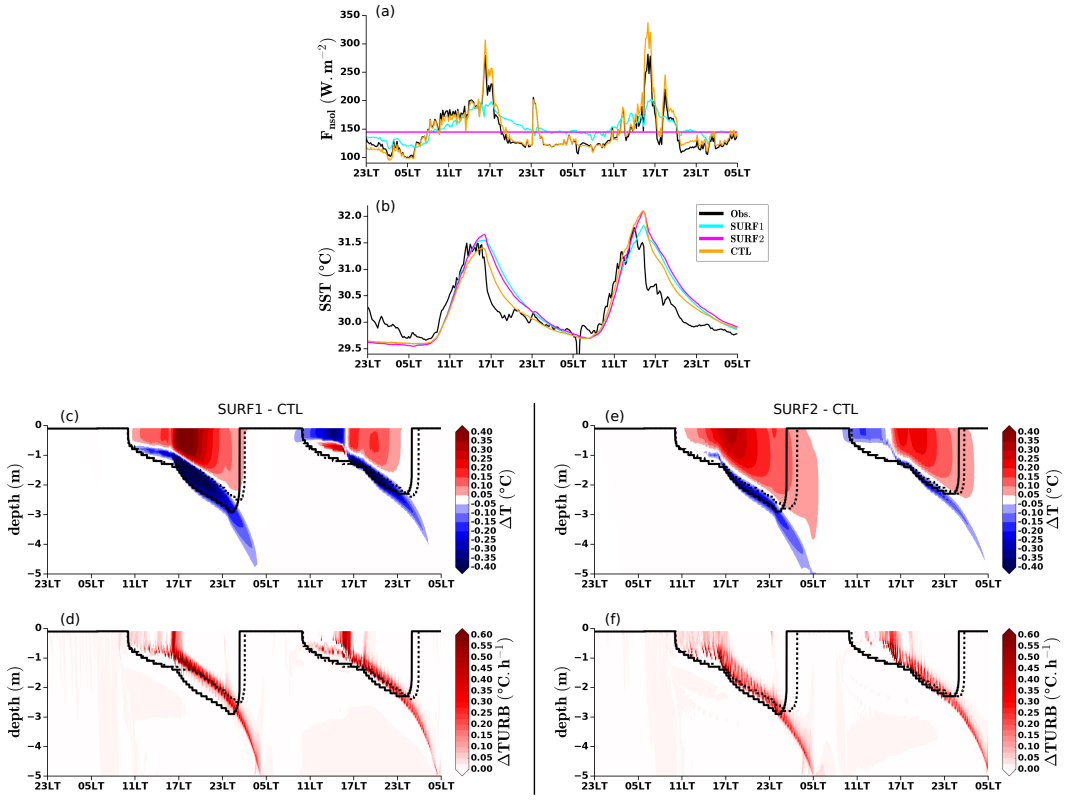

FIGURE 7 (a) Time series of the non-solar heating $F_{nsol} = LW_{up} - LW_{down} + LE + H$, (b) of the SST, and time-depth cross-sections of (c), (e) the difference of temperature and (d), (f) the difference of the vertical turbulent mixing $TURB$ (the second term of the right hand side in eq. 2) between the simulations listed in Table 2 and the reference simulation (CTL). The thick black contours represent the depth of the DWL for the reference (solid lines) and the test (dashed lines), respectively.

With no wind stress (D1), the DWL is thinner and warmer because it is limited to the solar flux penetrative layer (Fig. 6c). The wind stress greatly shapes the evolution of TKE, and no diurnal jet is simulated here compared to the reference simulation. This shows that the jet is generated through the wind-driven momentum. Increasing the wind stress at the surface (D2) results in larger TKE and shear at the base of the DWL (Fig. 6g and h), thus in a deeper DWL (Fig. 6f) and in a weaker SST diurnal cycle. A thinner and warmer (respectively deeper and cooler) DWL leads to a higher (respectively lower) SST amplitude.

3.2.3 | Surface cooling

The sensitivity tests performed here (Fig. 7) explore the impact of fixing the wind to its mean value over the period ($\overline{U_0}$ = 1.7 m s^{-1}; SURF1), or to fixing the non-solar flux to its mean value over the period ($\overline{F_{nsol}}$ = 146 W m^{-2}; SURF2).

Smoothing the non-solar heat flux, either directly (SURF2) or through the wind speed (SURF1) results in warmer SST and DWL (Fig. 7b and c). The temperature structure is particularly affected close to the peak of the non-solar heat flux with maximum temperature differences of 0.47 °C and 0.3 °C for SURF1 and SURF2, respectively. In both cases, the depth of the

DWL is only slightly affected. However, as expected less surface cooling leads to a warmer layer in SURF1.

The SURF2 test combines the effect of the temporal smoothing and of the absence of feedback between the SST and the non-solar heat fluxes, which are kept constant. The lack of energy loss in the afternoon (Fig. 7a) leads to a warmer DWL and longer (1 h 27 mn) DWL. The SST is higher, due to weaker surface cooling (Fig. 7b).

The SURF1 test impacts not only the non-solar heat fluxes but also the wind stress that governs the turbulent mixing. Additional sensitivity tests isolating the two contributions (not shown here) revealed that the final impact on the DWL is more due to the surface heat loss than to the wind stress, in agreement with the findings of Giglio et al. (2017). Here, the thinner and warmer DWL in the afternoon (Fig. 7c) is attributed to the reduction of the surface heat loss due to lighter wind with no gusts than to the reduction of the turbulent mixing (see also Fig. 7d).

We showed here than the 1-D oceanic model forced by the atmospheric R/V Revelle observations is able to accurately reproduce the observed DWL. We investigated the key processes involved in the evolution of the DWL and their sensitivity to the model formulations. The solar absorption is particularly sensitive to the formulation of the penetration profile and vertical discretization scheme. The DWL thickness and the amplitude of the SST variation are very sensitive to the wind stress amplitude. Suppressing the time variations of the non-solar heat fluxes inhibits the SST cooling and gives warmer DWL. Finally, suppressing the wind speed time variability impacts more the non-solar heat flux than the turbulent mixing, resulting in a thinner and warmer DWL.

4 | EVALUATION OF THE LARGE-EDDY SIMULATIONS WITH OBSERVATIONS

In order to investigate the evolution of the MABL above an oceanic DWL and to examine the coupling effects, an atmospheric LES has been performed for a 2-day period, coupled, at each surface grid point, with the 1-D oceanic model discussed in Sect. 3.1. This approach allows to represent the main ocean-atmosphere interactions.

4.1 | Air-Sea Exchanges

Figure 8 presents the temporal evolution of the surface parameters, i.e. SST, potential temperature θ_0, specific humidity q_0 and wind speed U_0 at z=10 m (the second level of the atmospheric model, to be comparable with the observations) and the associated air-sea exchanges through the turbulent surface fluxes (H, LE and τ), calculated from those thermodynamic parameters with the COARE 3.0 bulk parameterization. Considering the weak wind intensity, the advection of structures within the domain is relatively slow, which allows to compare here the spatial variability over the whole domain and the temporal variability observed at a fixed point on the R/V Revelle.

The SST diurnal cycle (Fig. 8a) is quite well reproduced by the coupled configuration. The SST seems almost spatially homogeneous over the simulation domain for the two days. The growing phase is correlated in time with the observations, with SST diurnal variations ranging 1.8–2.2 °C. For the second day, the simulated SST maximum is too high and slightly shifted in the afternoon, at around 1500 LT - 1600 LT, associated with an increase of the spatial variability. The too slow decay after sunset, already pointed out with the forced 1-D oceanic model, is still present in the coupled run. This discrepancy of the DWL dissipation is partly linked to the turbulent mixing inside the oceanic layer, the coupling being not able to improve it as inherent to the 1-D oceanic model. Compared to the results obtained with the forced 1-D oceanic run (cf. Sect. 3.1), the 1-D oceanic model in the coupled mode is also able to reproduce the evolution of the DWL and thus the diurnal cycle of the SST. Interestingly, during

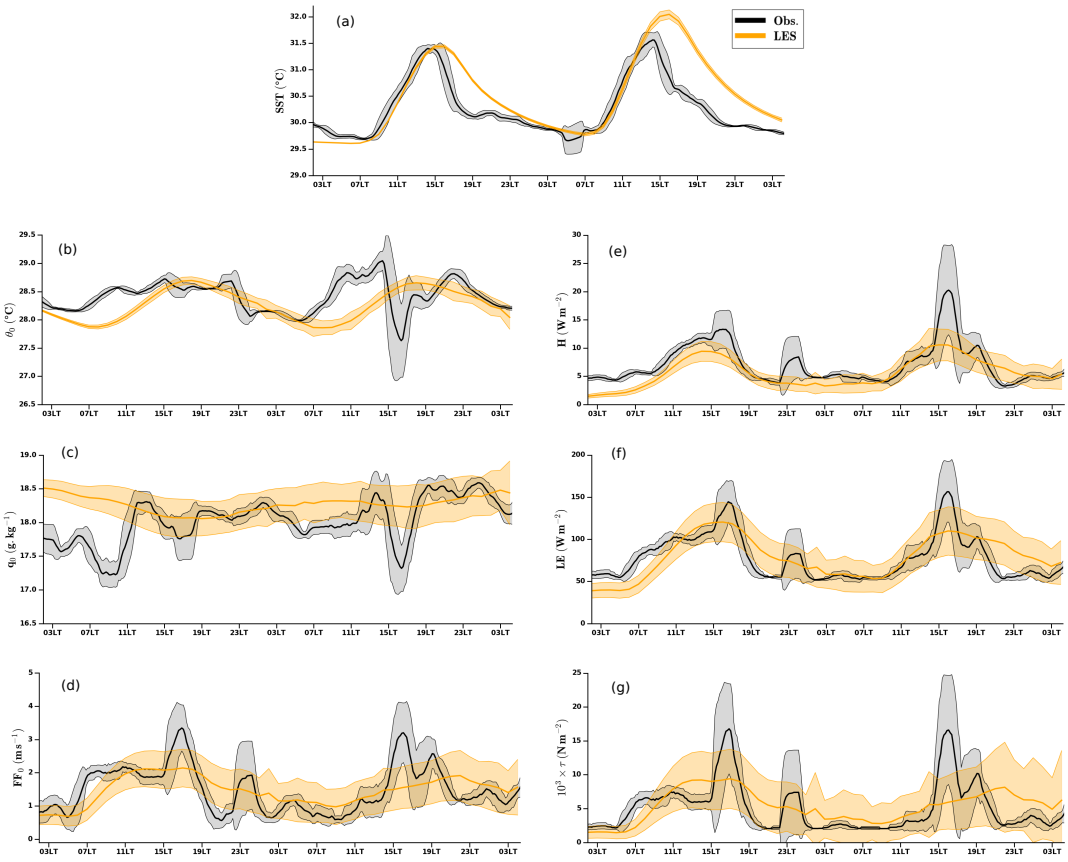

FIGURE 8 Mean and +/− standard deviation time series of (a) sea surface temperature (SST), (b) potential temperature (θ_0), (c) specific humidity (q_0), (d) wind speed (U_0) close to the surface, taken at the second level of the atmospheric model (i.e. 10 m), (e) sensible heat flux (H), (f) latent heat flux (LE) and (g) surface wind stress (τ). For the coupled LES (orange lines), the mean and the standard deviations are calculated on hourly output over the whole domain. For the R/V Revelle observations (black lines), the mean and standard deviation are calculated over a 2h sliding interval. The turbulent fluxes are computed with the COARE 3.0 bulk algorithm.

nighttime, at the R/V Revelle, a SST drop is monitored around 0600 LT for 10 to 20 minutes. As no substantial temperature changes are observed on the Chameleon profiles (Fig 1c), a shallow cold rain layer is expected. Considering the extreme values, the simulation presents some rare low values of SST consistent with the cold value observed.

The temporal evolution of the atmospheric potential temperature close to the surface are reproduced by the LES (Fig. 8b) with a well-marked diurnal cycle. The atmospheric specific humidity close to the surface (Fig. 8c) does not exhibit a pronounced diurnal cycle, consistently with the observations. The coupled LES leads to an almost constant standard deviation of surface potential temperature and specific humidity throughout the duration of the simulation while the observations present more variability, especially around 1600 LT on the second day. The time series of the surface wind speed in Fig. 8d presents a weak diurnal cycle, correctly reproduced by the LES; remember however that in the simulation the wind is nudged towards observed wind with a relaxation timescale of 3 hours (cf. Sect. 2.2.3). Even if the wind conditions are very light, the spatial variability of the simulated surface wind speed is relatively large and almost constant with time. The sharp peak of U_0 observed around 1600

LT is supposed to be related to convective gusts (Bellenger et al., 2010). Indeed, the observed rain event (see Fig. 12 below) around 1530 LT is time-correlated with a drop in potential temperature (Fig. 8b), which supports the hypothesis of a cold pool occurrence. This localized event observed at the R/V Revelle is not reproduced by the atmospheric LES, however the positively skewed distribution in U_0 and the negatively skewed distribution of θ_0 (not shown here) may trace the existence of cold pools.

As expected from an adequate simulation of SST, θ_0, q_0 and U_0, the surface sensible and latent heat fluxes as well as the wind stress are close to observations (Fig. 8e, f and g). As U_0 is one of the key parameters for the computation of the turbulent surface fluxes, their spatial variability is mainly induced by the surface wind speed. The coupled framework, an atmospheric LES coupled with an 1-D oceanic model, is thus able to correctly reproduce the air–sea exchanges associated to the presence of a diurnal warm layer.

4.2 | Marine Atmospheric Boundary Layer Structure

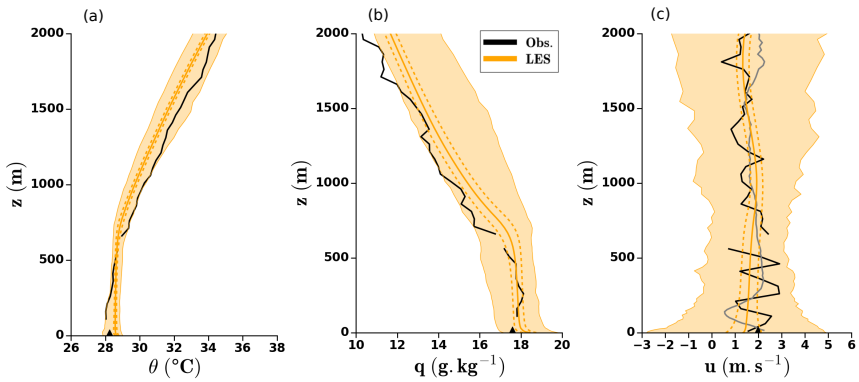

FIGURE 9 Vertical profiles of (a) potential temperature, (b) specific humidity and (c) wind speed averaged over the LES horizontal domain (solid lines) +/− the standard deviation (dashed lines) the 15 nov. at 1700 LT, after 42 hours of simulation. The coloured zones represent the full range of simulated profiles over the domain. The orange lines are the atmospheric LES coupled with a 1-D oceanic model, the black and gray lines correspond to the radiosounding launched from the R/V Revelle the 15 nov. at 1709LT and the wind from the Lidar profiler, respectively. The black triangles refer to the surface R/V Revelle observations at $z \sim 10$ m. The

The vertical MABL structure reproduced by the LES, after 42 hours of simulation, is compared to profiles recorded by the R/V Revelle radiosounding and Lidar observations at 1709 LT. The full range of potential temperature, specific humidity and wind speed profiles and their corresponding mean profiles are shown in Fig. 9. The simulated profiles of potential temperature are almost homogeneous over the whole domain and in good agreement with the R/V Revelle's radiosounding. The mean value of specific humidity in the simulated MABL is also consistent with the observed radiosounding. However, the humidity variability is more significant (as already shown in Fig. 8c), especially above the MABL where the simulated air masses are slightly too wet, with a range of values at the edge of the observations. The spatial variability of the wind is significant over the whole MABL as already shown in Fig. 8d but the mean value is consistent with the observations from the radiosounding and from the Lidar.

The time evolution of the MABL depth, mean potential temperature and specific humidity is presented in Fig. 10 confirming results shown in Fig. 9 for a given time. The boundary-layer depth, z_i, is estimated from the radiosounding following the subjective procedure used in Johnson and Ciesielski (2017) where z_i is the level identified by an abrupt increase in stability and

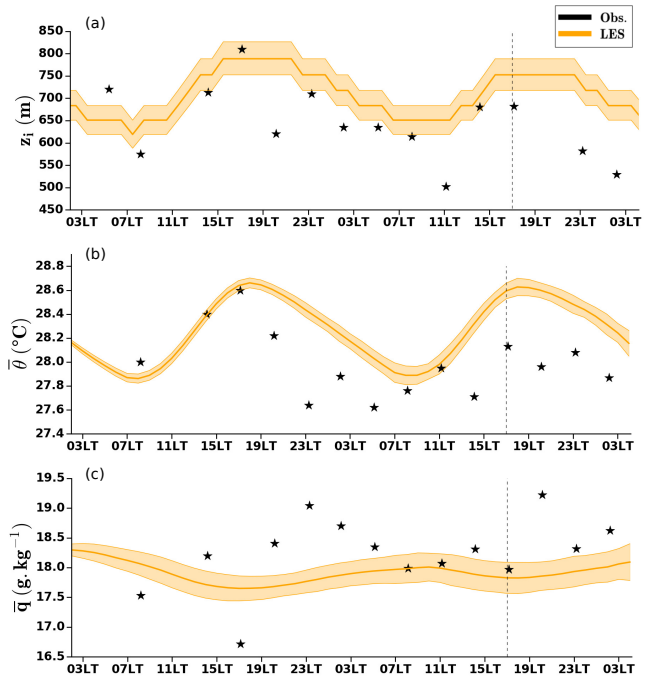

FIGURE 10 Time series of MABL (a) depth (z_i), (b) potential temperature ($\overline{\theta}$) and (c) specific humidity ($\overline{q}$) in the LES coupled with a 1-D oceanic model. The solid lines referred to averaged values over the whole MABL. For the estimate of z_i, the coloured area represents precision associated to the vertical grid ($z_i \pm \Delta z$) and the standard deviation intervals for θ and q. The black stars correspond to observed values estimated from the R/V Revelle radiosoundings. The vertical black dashed line indicates the time at which the MABL profiles are shown in Fig. 9.

an abrupt decrease in humidity. The simulated MABL depth is defined as the height of the minimum of domain-average vertical buoyancy flux (Deardorff, 1972). Throughout the two days of simulation, the boundary-layer depth and the mean potential temperature are similar to observations with an increase of the boundary-layer depth and potential temperature during daytime following the increase of SST. The temporal evolution of the mean specific humidity is less accurately simulated with smoother variations than the observations. The MABL submitted to a diurnal cycle of SST, resulting from coupling with an 1-D oceanic model, evolves similarly to previous results using observations Johnson and Ciesielski (2017) or simulations by Ruppert and Johnson (2016), with an afternoon mixed-layer warming of around 0.8 °C, a drying of around 0.5 g kg^{-1} associated with a deepening of around 140 m. Here, we can also note that the simulated MABL is slightly warmer, drier and thicker than the observations. The coupled LES correctly reproduces the mean observed characteristics of the MABL including boundary-layer depth, potential temperature, specific humidity and wind speed.

Once the mean MABL structure has been validated, the time evolution of turbulence and cloud fields is then investigated. The horizontal cross-sections of 100 m-vertical velocity and 10 m-virtual potential temperature fluctuations (i.e. removing the domain mean average) are shown in Fig. 11a and Fig. 11b. The turbulence field appears to be organized into open cells defined by the vigorous updrafts along the edges of the cells and weaker downdrafts inside the cells. As suggested by Ruppert and Johnson (2015) and Rowe and Houze Jr. (2015), the light wind conditions during the MJO suppressed phase of November 2011 are favourable to a mesoscale organization into open cells rather than convective rolls. The rain water path (RWP) field presented in Fig. 11c shows the existence of various rainy cells. Associated to those rainy cells, the virtual potential temperature

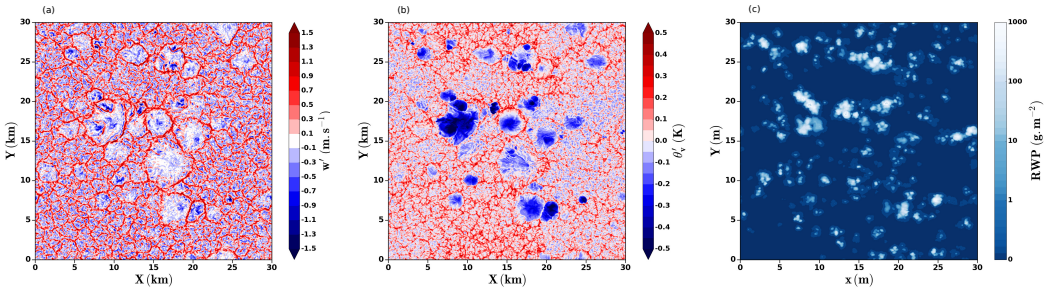

FIGURE 11 Horizontal cross-sections the 15 nov. at 1700 LT of (a) the vertical velocity component fluctuations (w') at 100 m, (b) the virtual potential temperature fluctuations (θ'_v) at 10 m and (c) the rain water path (RWP).

and vertical velocity fluctuations also show larger patches of negative values. This is a signature of cold pools triggered by the descent of cold air down to the surface due to the evaporation of rain drops into an unsaturated environment. Those cold pools spread at the surface and induce upward motions all around well visible in Fig. 11a in particular on the center of the domain. Those structures are consistent with previous studies, such as, Feng et al. (2015), Rowe and Houze Jr. (2015), Skyllingstad and de Szoeke (2015) which were rather associated with deep convection. Feingold et al. (2010) using satellite images and LES simulations showed how precipitating clouds produce an open cellular cloud pattern that oscillates between different, weakly stable states. Due to different present environmental conditions, the convection is weaker than in these previous studies, and leads to weak rainfall and cold pool intensity as suggested by Zuidema et al. (2012) which focused on cold pools associated to shallow convection.

The turbulence activity presents a well-marked diurnal cycle as shown in Fig. 12a and Fig. 12b with a larger spread of the 100 m-vertical velocity and 10 m-virtual potential temperature fluctuations during daytime. The box and whiskers plot representation reveals extreme values of virtual potential temperature fluctuations more negative than -0.5 K and of vertical velocity fluctuations more negative than -1 m s^{-1} which correspond to the cold pool values.

In the case of the LES simulation coupled with the 1-D oceanic model, the downdraft shortwave flux is simulated and no longer prescribed from observations as it was the case for the forced 1-D oceanic configuration. As shown in Fig. 12c, the domain-average shortwave flux is close to the radiometer's observation at the R/V Revelle, but there are locally areas where SW_{down} is very low, even close to zero, which highlights the presence of clouds and their impact on the downward solar flux actually reaching the surface of the ocean.

Rainfall is also present in the coupled LES as illustrated in Fig. 12d even if the atmospheric convection is not deep. The coupled LES is then able to reproduce the associated structures to this shallow cumulus activity with the signature of cold pools already highlighted on the surface parameters and on the turbulent activity. At the R/V Revelle, only a localized rain event has been monitored the 15 nov. after 1530 LT which can explain the surface wind gust and the fall of surface temperature at 1600LT observed in Fig. 8. This spatially-localized cold pool process, observed here at a fixed point, is also reproduced by the coupled LES at various areas of the domain.

Figure 12e presents the temporal evolution of the cloud cover. There is a distinct diurnal cycle of the cloud base which is strongly correlated to the MABL daytime evolution. The cloud layer is thus strongly linked to the SST and driven by the turbulent surface fluxes. The evolution of the cloud fraction reflects a daytime cumulus growth with a wider covered surface and a deepening of clouds from the sunrise to the late afternoon. Those results are consistent with previous studies on the diurnal cycle of the cumulus convection (Ruppert and Johnson, 2015, 2016). Present results confirm simulation results of Ruppert and Johnson (2016), using horizontally homogeneous prescribed SST. The observations obtained from the ceilometer show a light occurrence of cumulus above the R/V Revelle, which is consistent with the low values of simulated cloud fraction (below 5%).

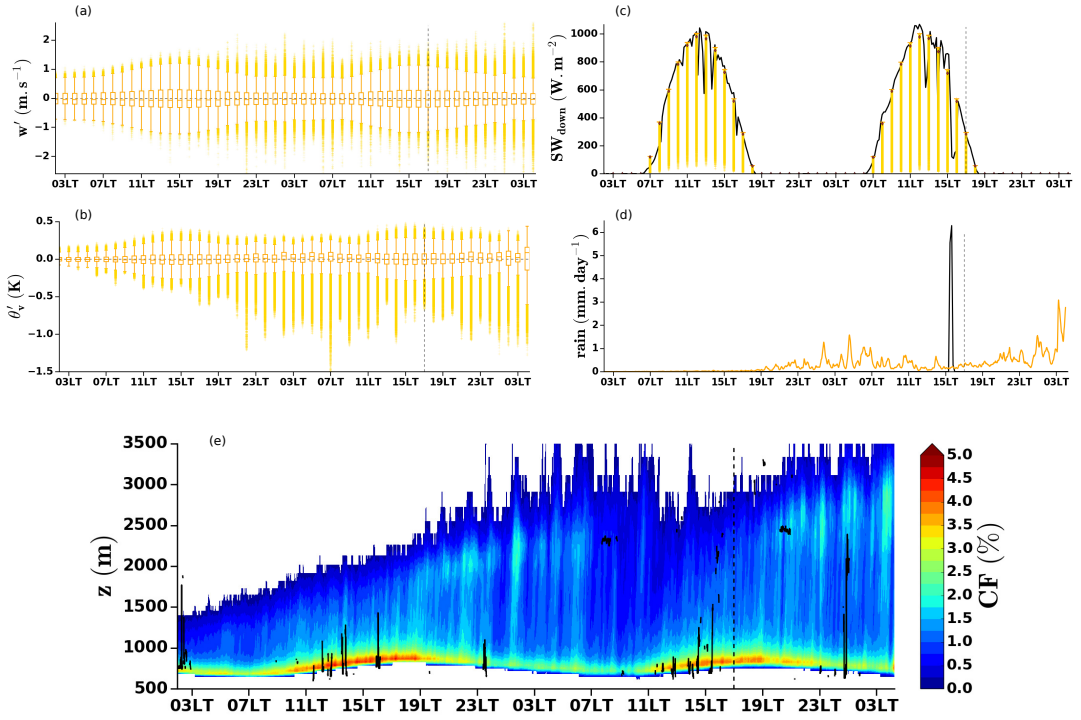

FIGURE 12 Box and whiskers plots of (a) the 100 m-vertical velocity component fluctuations (w') , (b) the 10 m-virtual potential temperature fluctuations (θ'_v) and (c) the downward shortwave radiation (SW_{down}). The center line of a box plot indicates the median value, the edges of the box are the interquartile ranges and the yellow stars are the extreme value. (d) The time serie of the domain-averaged rainfall simulated in the coupled LES (orange line) and observed rainfall at the R/V Revelle (black line) and (e) the time-height cross-section of the simulated cloud fraction with the observed cloud base estimates from the ceilometer (in black). The vertical black dashed line indicates the time the time at which the horizontal cross-sections are represented in Fig. 11.

Over the periods of highest cloud cover i.e. between 1100 LT and 1700 LT, the simulated cloud base is in agreement with the estimates of the observed cloud base.

5 | DISCUSSION AND CONCLUSIONS

Based on atmospheric and oceanic observations collected during the DYNAMO field campaign, a case study has been built to examine the ocean-atmosphere interactions during the occurrence of a DWL. We have selected a period of 54 hours, between the 13 nov. and the 15 nov. 2011, with favourable atmospheric conditions for the formation of a DWL, i.e. MJO suppressed phase, clear sky conditions, high solar radiations and light surface wind speed. This coupled case study is now available to realize more numerical studies to analyze the ocean-atmosphere interactions when DWL is present, as well as their representation in models from LES to Single-Column models. In the present paper, a 1-D oceanic model and an atmospheric LES coupled with the same 1-D oceanic model have been used.

The 1-D oceanic model with high vertical resolution is able to reproduce the DWL behaviour over the 2-day period. The

model is constrained at the surface by observed atmospheric fields issued from the R/V Revelle. The key processes involved in the DWL life cycle have then been examined with sensitivity tests. The solar radiation absorption is the main source of the DWL growth. To be properly taken into account, the absorption coefficients should be carefully chosen to fit the current situation and its numerical discretization done with care. The importance of surface stress for the representation of the diurnal oceanic jet, and consequently for the turbulent vertical mixing induced by the shear instabilities as the deepening of the DWL occurs has been highlighted using various surface stresses. At the air-sea interface, the oceanic layer loses energy through the non-solar heating flux composed of the sensible, latent and net longwave radiative fluxes. An accurate representation of this surface cooling is necessary to represent the temporal extension and the intensity of the DWL and consequently the evolution of the SST. As the predicted SST is explicitly used for the computation of the non-solar flux contributing to the surface cooling, several non-linear relationships between the involved mechanisms lead to complex interplays. The 1-D oceanic model is to a reasonable extent able to realistically reproduce the evolution of a DWL. Of course, some deficiencies remain, especially with regard to the SST decay phase in the afternoon. One area for improvement could be the adjustment of the turbulence scheme in the oceanic mixed layer in order to be adapted to these stable stratification conditions. For this purpose, an outcome of the present work, an oceanic LES would be a relevant approach.

An atmospheric LES model coupled with the 1-D oceanic model previously validated, has then be used to investigate how the presence of a DWL influence the MABL structure. This simulation has been evaluated against available observations and is found to provide a general behaviour of the evolution of the MABL in agreement with observations, namely its thickness and thermodynamical structure. The simulated turbulence field is organized into open-cells with vigorous thermals along the edge of the cells; the occurrence of cold pools associated to precipitating shallow cumulus is also simulated consistent with observations. The shallow cumulus convection appears to be directly rooted to the air-sea exchanges and the presence of a DWL leads to a diurnal cycle of the cloud layer. The cloud base thus closely follows the MABL depth daytime evolution associated with a larger cloud cover and a deepening of the clouds in the late afternoon.

Coupling atmospheric LES with the 1-D oceanic model allows to represent the main interactions between the ocean and the atmosphere and to simulate a spatial variability of SST and therefore of air-sea exchanges. Such work could pave the way to investigate the tight interplay between the oceanic mixed layer structure, the air-sea interaction, the mesoscale organization of turbulent thermals and shallow clouds.

The build up of this numerical case study with a 1-D – LES coupling is a first achievement. The next step is to use it to evaluate the coupled ocean-atmosphere models in a Single-Column Model framework, following the methodology developed in the GEWEX Cloud Systems Studies (GCSS) project (Siebesma et al., 2003; vanZanten et al., 2011) and the GEWEX Atmospheric Boundary Layer Study (GABLS) project (Beare et al., 2006) where regional or global model are compared to LES used as a reference as first proposed by Randall et al. (1996). A second major perspective will be the design of an ocean LES - atmosphere LES coupling framework in order to reproduce explicitly the oceanic turbulent processes and the spatial structure of a DWL. In particular, this would allow to better understand the oceanic turbulent vertical transport under stably stratified conditions and to improve the oceanic turbulent schemes.

ACKNOWLEDGEMENTS

This work was supported by the French national research agency (Agence National de la Recherche) through the ANR-COCOA project “COmprehensive Coupling approach for the Ocean and the Atmosphere” (grant: ANR-16-CE01-0007). Data used in this research, from the DYNAMO field campaign, are provided by NCAR/EOL under the sponsorship of the National Science Foundation and are available on the DYNAMO website (`https://www.eol.ucar.edu/field_projects/dynamo`). We would like to thank H. Bellenger (LMD) for the constructive discussions about the diurnal warm layer processes, F. Lemarié

(Inria) for its expertise on numerical modelling. We also gratefully thank J. Moum (OSU), C. Fairall (NOAA) and L. Bariteau (NOAA) for providing details about the observations of the oceanic layer and of the surface turbulent fluxes.

APPENDIX A: LARGE SCALE VERTICAL VELOCITY FORCING

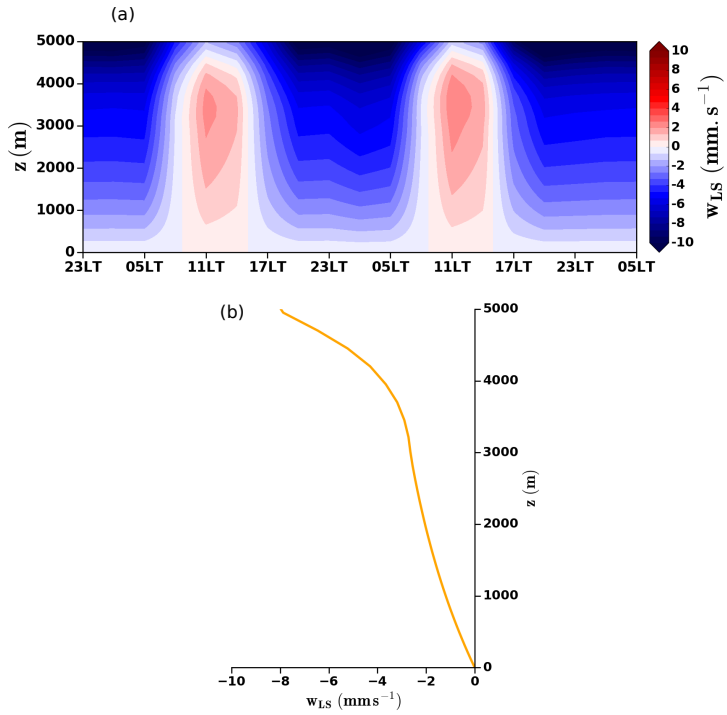

FIGURE 13 (a) Time-height cross-section of the large–scale vertical velocity field from an radiative-convective equilibrium (see appendix A for details) and (b) vertical profile of the large–scale vertical velocity averaged over the 54 h interval selected for the simulation.

The large–scale vertical velocity has been estimated using a radiative–convective equilibrium assumption (Sobel and Bretherton, 2000; Mapes, 2001). Above the MABL, where the turbulent intensity becomes negligible, the diabatic radiative effects (cooling or warming) and the adiabatic motions (Sobel et al., 2001) balanced each other. The junction function proposed by Bellon and Stevens (2012), an exponential interpolation, is applied between the profile of $w_{LS}(z)$ above the MABL and the surface limit condition $w_{LS}(z = 0) = 0$. Figure 13a presents the time–height cross–section of the large–scale vertical velocity for the entire period of the simulation. The diurnal evolution of w_{LS} is closely linked to the radiative cooling or warming. The subsidence is enhanced during the night while after sunrise, the increase of shortwave radiation leads to an opposite sign of the vertical velocity with ascending motion that remains weak compared to the subsidence with values of around 2.5 mm s^{-1} and -7.2 mm s^{-1} at 4000 m, respectively. The evolution of w_{LS} is consistent with previous studies such as Johnson et al. (2015) based on a sounding network during DYNAMO field campaign or Ruppert and Johnson (2016) using the weak temperature gradient (WTG) scheme to compute the large–scale vertical velocity. As observed during the DYNAMO field campaign, inhibited

convection regimes lead to atmospheric conditions quite similar from one day to the next, the diurnal evolution of the large–scale vertical velocity is thus very similar for the two days of interest. Sensitivity numerical tests with the model, show that the diurnal cycle of w_{LS} had a small impact of results. Therefore, to keep as much simple the simulations, a constant-in-time profile of vertical velocity (Fig 13b) is prescribed. In a daily-mean point of view, the large scale vertical velocity reflects a subsidence motion. This is relevant of a present MJO suppressed phase. This large–scale subsidence, which partly controls the moistening of the MABL, contributes to inhibit the moist convective activity. (Takemi et al., 2004; Ruppert and Johnson, 2015)

REFERENCES

Robert J. Beare, Malcolm K. Macvean, Albert A. M. Holtslag, Joan Cuxart, Igor Esau, Jean-Christophe Golaz, Maria A. Jimenez, Marat Khairoutdinov, Branko Kosovic, David Lewellen, Thomas S. Lund, Julie K. Lundquist, Anne Mccabe, Arnold F. Moene, Yign Noh, Siegfried Raasch, and Peter Sullivan. An intercomparison of large-eddy simulations of the stable boundary layer. *Boundary-Layer Meteorology*, 118(2):247–272, 2006. doi: https://doi.org/10.1007/s10546-004-2820-6.

H. Bellenger, Y. N. Takayabu, T. Ushiyama, and K. Yoneyama. Role of Diurnal Warm Layers in the Diurnal Cycle of Convection over the Tropical Indian Ocean during MISMO. *Monthly Weather Review*, 138(6):2426–2433, June 2010. doi: https://doi.org/10.1175/2010MWR3249.1.

Hugo Bellenger and Jean-Philippe Duvel. An Analysis of Tropical Ocean Diurnal Warm Layers. *Journal of Climate*, 22(13):3629–3646, July 2009. doi: https://doi.org/10.1175/2008JCLI2598.1.

Gilles Bellon and Bjorn Stevens. Using the sensitivity of large-eddy simulations to evaluate atmospheric boundary layer models. *Journal of the Atmospheric Sciences*, 69(5):1582–1601, 2012. doi: https://doi.org/10.1175/JAS-D-11-0160.1.

D. J. Bernie, S. J. Woolnough, J. M. Slingo, and E. Guilyardi. Modeling Diurnal and Intraseasonal Variability of the Ocean Mixed Layer. *Journal of Climate*, 18(8):1190–1202, April 2005. doi: https://doi.org/10.1175/JCLI3319.1.

D. J. Bernie, E. Guilyardi, G. Madec, J. M. Slingo, S. J. Woolnough, and J. Cole. Impact of resolving the diurnal cycle in an ocean–atmosphere GCM. Part 2: A diurnally coupled CGCM. *Climate Dynamics*, 31(7-8):909–925, December 2008. doi: https://doi.org/10.1007/s00382-008-0429-z.

Sandrine Bony and Bjorn Stevens. Measuring Area-Averaged Vertical Motions with Dropsondes. *Journal of the Atmospheric Sciences*, 76(3):767–783, March 2019. doi: https://doi.org/10.1175/JAS-D-18-0141.1.

Kenneth P. Bowman, J. Craig Collier, Gerald R. North, Qiaoyan Wu, Eunho Ha, and James Hardin. Diurnal cycle of tropical precipitation in Tropical Rainfall Measuring Mission (TRMM) satellite and ocean buoy rain gauge data. *Journal of Geophysical Research*, 110 (D21), 2005. doi: https://doi.org/10.1029/2005JD005763.

A. Brewer. R/V Roger Revelle High Resolution Doppler Lidar (HRDL) Data. Version 1.0, 2013. Artwork Size: 2 data files, 196 MiB Medium: NetCDF: Network Common Data Form (application/x-netcdf) Pages: 2 data files, 196 MiB Version Number: 1.0 type: dataset.

Pierre-Etienne Brilouet, Pierre Durand, and Guylaine Canut. The Marine Atmospheric Boundary Layer Under Strong Wind conditions: Organized Turbulence Structure and Flux Estimates by Airborne Measurements. *Journal of Geophysical Research: Atmospheres*, 122(4):2115–2130, February 2017. URL http://doi.wiley.com/10.1002/2016JD025960.

Pierre-Etienne Brilouet, Pierre Durand, Guylaine Canut, and Nadia Fourrié. Organized turbulence in a cold-air outbreak: Evaluating a large-eddy simulation with respect to airborne measurements. *Boundary-Layer Meteorology*, 2019. doi: https://doi.org/10.1007/s10546-019-00499-4.

Michael A. Brunke, Chris W. Fairall, Xubin Zeng, Laurence Eymard, and Judith A. Curry. Which Bulk Aerodynamic Algorithms are Least Problematic in Computing Ocean Surface Turbulent Fluxes? *Journal of Climate*, 16(4):619–635, February 2003. URL https://doi.org/10.1175/1520-0442(2003)016\T1\textless0619:WBAAAL\T1\textgreater2.0.CO;2.

D. R. Caldwell, R-C. Lien, J. N. Moum, and M. C. Gregg. Turbulence Decay and Restratification in the Equatorial Ocean Surface Layer following Nighttime Convection. *Journal of Physical Oceanography*, 27(6):1120–1132, June 1997. doi: https://doi.org/10.1175/1520-0485(1997)027\textless1120:TDARIT\textgreater2.0.CO;2.

Paul E. Ciesielski, Hungjui Yu, Richard H. Johnson, Kunio Yoneyama, Masaki Katsumata, Charles N. Long, Junhong Wang, Scot M. Loehrer, Kathryn Young, Steven F. Williams, William Brown, John Braun, and Teresa Van Hove. Quality-Controlled Upper-Air Sounding Dataset for DYNAMO/CINDY/AMIE: Development and Corrections. *Journal of Atmospheric and Oceanic Technology*, 31(4):741–764, April 2014. doi: 10.1175/JTECH-D-13-00165.1.

Carol Anne Clayson and Derrick Weitlich. Variability of tropical diurnal sea surface temperature. *Journal of Climate*, 20(2):334–352, 2007. doi: https://doi.org/10.1175/JCLI3999.1.

Phillip Colella and Paul R Woodward. The piecewise parabolic method (ppm) for gas-dynamical simulations. *Journal of Computational Physics*, 54(1):174 – 201, 1984. ISSN 0021-9991. doi: https://doi.org/10.1016/0021-9991(84)90143-8. URL http://www.sciencedirect.com/science/article/pii/0021999184901438.

Meghan F. Cronin and William S. Kessler. Near-Surface Shear Flow in the Tropical Pacific Cold Tongue Front*. *Journal of Physical Oceanography*, 39(5):1200–1215, May 2009. doi: https://doi.org/10.1175/2008JPO4064.1.

J. Cuxart, P. Bougeault, and J.-L. Redelsperger. A turbulence scheme allowing for mesoscale and large-eddy simulations. *Quarterly Journal of the Royal Meteorological Society*, 126(562):1–30, January 2000. ISSN 00359009, 1477870X. URL http://doi.wiley.com/10.1002/qj.49712656202.

Stephan R. de Roode, Peter G. Duynkerke, and Harm J. J. Jonker. Large-Eddy Simulation: How Large is Large Enough? *Journal of the Atmospheric Sciences*, 61(4):403–421, February 2004. doi: https://doi.org/10.1175/1520-0469(2004)061\textless0403:LSHLIL\textgreater2.0.CO;2.

Simon P. de Szoeke, James B. Edson, June R. Marion, Christopher W. Fairall, and Ludovic Bariteau. The MJO and Air–Sea Interaction in TOGA COARE and DYNAMO. *Journal of Climate*, 28(2):597–622, January 2015. doi: https://doi.org/10.1175/JCLI-D-14-00477.1.

James W. Deardorff. Parameterization of the Planetary Boundary layer for Use in General Circulation Models. *Monthly Weather Review*, 100(2):93–106, February 1972. doi: https://doi.org/10.1175/1520-0493(1972)100\textless0093:POTPBL\textgreater2.3.CO;2.

James W. Deardorff. Stratocumulus-capped mixed layers derived from a three-dimensional model. *Boundary-Layer Meteorology*, 18 (4):495–527, Jun 1980. doi: 10.1007/BF00119502.

Peter G. Duynkerke, Stephan R. de Roode, Margreet C. van Zanten, Javier Calvo, Joan Cuxart, Sylvain Cheinet, Andreas Chlond, Hervé Grenier, Piet J. Jonker, Martin Köhler, Geert Lenderink, David Lewellen, Cara-Lyn Lappen, Adrian P. Lock, Chin-Hoh Moeng, Frank Müller, Dolores Olmeda, Jean-Marcel Piriou, Enrique Sánchez, and Igor Sednev. Observations and numerical simulations of the diurnal cycle of the EUROCS stratocumulus case. *Quarterly Journal of the Royal Meteorological Society*, 130(604):3269–3296, October 2004. doi: https://doi.org/10.1256/qj.03.139.

Earth Observing Laboratory. R/V Roger Revelle Radiosonde L3.1 Data. Version 1.0, 2014. Artwork Size: 136 data files, 1 ancillary/documentation file, 390 MiB Medium: EOL Sounding Composite Format (ASCII) Pages: 136 data files, 1 ancillary/documentation file, 390 MiB Version Number: 1.0 type: dataset.

C. W. Fairall, E. F. Bradley, D. P. Rogers, J. B. Edson, and G. S. Young. Bulk parameterization of air-sea fluxes for Tropical Ocean-Global Atmosphere Coupled-Ocean Atmosphere Response Experiment. *Journal of Geophysical Research: Oceans*, 101(C2):3747–3764, February 1996. doi: https://doi.org/10.1029/95JC03205.

C. W. Fairall, E. F. Bradley, J. E. Hare, A. A. Grachev, and J. B. Edson. Bulk Parameterization of Air–Sea Fluxes: Updates and Verification for the COARE Algorithm. *Journal of Climate*, 16(4):571–591, February 2003. ISSN 0894-8755, 1520-0442. URL https://doi.org/10.1175/1520-0442(2003)016<0571:BPOASF>2.0.CO;2.

Graham Feingold, Ilan Koren, Hailong Wang, Huiwen Xue, and Wm Alan Brewer. Precipitation-generated oscillations in open cellular cloud fields. *Nature*, 466(7308):849–852, 2010. doi: https://doi.org/10.1038/nature09314.

Zhe Feng, Samson Hagos, Angela K. Rowe, Casey D. Burleyson, Matus N. Martini, and Simon P. de Szoeke. Mechanisms of convective cloud organization by cold pools over tropical warm ocean during the AMIE/DYNAMO field campaign. *Journal of Advances in Modeling Earth Systems*, 7(2):357–381, June 2015. doi: https://doi.org/10.1002/2014MS000384.

G. Flato, J. Marotzke, B. Abiodun, P. Braconnot, S. C. Chou, W. Collins, P. Cox, F. Driouech, S. Emori, V. Eyring, C. Forest, P. Gleckler, E. Guilyardi, C. Jakob, V. Kattsov, C. Reason, and M. Rummukainen. *Evaluation of climate models*, pages 741–882. Cambridge University Press, Cambridge, UK, 2013. doi: https://doi.org/10.1017/CBO9781107415324.020.

Philippe Gaspar, Yves Grégoris, and Jean-Michel Lefevre. A simple eddy kinetic energy model for simulations of the oceanic vertical mixing: Tests at station Papa and long-term upper ocean study site. *Journal of Geophysical Research: Oceans*, 95(C9):16179–16193, 1990. ISSN 2156-2202. URL http://dx.doi.org/10.1029/JC095iC09p16179.

Donata Giglio, Sarah T. Gille, Aneesh C. Subramanian, and San Nguyen. The role of wind gusts in upper ocean diurnal variability. *Journal of Geophysical Research: Oceans*, 122(9):7751–7764, 2017. doi: https://doi.org/10.1002/2017JC012794.

D. Gregory, J.-J. Morcrette, C. Jakob, A. C. M. Beljaars, and T. Stockdale. Revision of convection, radiation and cloud schemes in the ecmwf integrated forecasting system. *Quarterly Journal of the Royal Meteorological Society*, 126(566):1685–1710, 2000. doi: https://doi.org/10.1002/qj.49712656607.

Madec Gurvan, Romain Bourdallé-Badie, Jérôme Chanut, Emanuela Clementi, Andrew Coward, Christian Ethé, Doroteaciro Iovino, Dan Lea, Claire Lévy, Tomas Lovato, Nicolas Martin, Sébastien Masson, Silvia Mocavero, Clément Rousset, Dave Storkey, Martin Vancoppenolle, Simon Müeller, George Nurser, Mike Bell, and Guillaume Samson. Nemo ocean engine, October 2019. Add SI3 and TOP reference manuals.

Yoo-Geun Ham, Jong-Seong Kug, In-Sik Kang, Fei-Fei Jin, and Axel Timmermann. Impact of diurnal atmosphere–ocean coupling on tropical climate simulations using a coupled GCM. *Climate Dynamics*, 34(6):905–917, May 2010. doi: https://doi.org/10.1007/s00382-009-0586-8.

X. Jiang, A. Adames, D. Kim, E. Maloney, H. Lin, H. Kim, C. Zhang, C. Demott, and N. Klingaman. Fifty years of research on the madden-julian oscillation: Recent progress, challenges, and perspectives. *Journal of Geophysical Research: Atmospheres*, page e2019JD030911, 07 2020. doi: 10.1029/2019JD030911.

Richard H. Johnson and Paul E. Ciesielski. Multiscale Variability of the Atmospheric Boundary Layer during DYNAMO. *Journal of the Atmospheric Sciences*, 74(12):4003–4021, December 2017. doi: https://doi.org/10.1175/JAS-D-17-0182.1.

Richard H. Johnson, Paul E. Ciesielski, and Jennifer A. Cotturone. Multiscale Variability of the Atmospheric Mixed Layer over the Western Pacific Warm Pool. *Journal of the Atmospheric Sciences*, 58(18):2729–2750, September 2001. doi: https://doi.org/10.1175/1520-0469(2001)058\textless2729:MVOTAM\textgreater2.0.CO;2.

Richard H. Johnson, Paul E. Ciesielski, James H. Ruppert, and Masaki Katsumata. Sounding-Based Thermodynamic Budgets for DYNAMO. *Journal of the Atmospheric Sciences*, 72(2):598–622, February 2015. doi: https://doi.org/10.1175/JAS-D-14-0202.1.

Ioanna Karagali, Jacob L. Høyer, and Craig J. Donlon. Using a 1-d model to reproduce the diurnal variability of sst. *Journal of Geophysical Research: Oceans*, 122(4):2945–2959, 2017. doi: https://doi.org/10.1002/2016JC012542.

Yoshimi Kawai and Akiyoshi Wada. Diurnal sea surface temperature variation and its impact on the atmosphere and ocean: A review. *Journal of Oceanography*, 63(5):721–744, October 2007. doi: https://doi.org/10.1007/s10872-007-0063-0.

Edwin Kessler. On the Distribution and Continuity of Water Substance in Atmospheric Circulations. In *On the Distribution and Continuity of Water Substance in Atmospheric Circulations*, pages 1–84. American Meteorological Society, 1969. ISBN 978-1-935704-36-2. doi: https://doi.org/10.1007/978-1-935704-36-2_1.

Marat Khairoutdinov and David Randall. High-Resolution Simulation of Shallow-to-Deep Convection Transition over Land. *Journal of the Atmospheric Sciences*, 63(12):3421–3436, December 2006. doi: https://doi.org/10.1175/JAS3810.1.

Vladimir N. Kudryavtsev and Alexander V. Soloviev. Slippery Near-Surface Layer of the Ocean Arising Due to Daytime Solar Heating. *Journal of Physical Oceanography*, 20(5):617–628, May 1990. doi: https://doi.org/10.1175/1520-0485(1990)020\textless0617:SNSLOT\textgreater2.0.CO;2.

C. Lac, J.-P. Chaboureau, V. Masson, J.-P. Pinty, P. Tulet, J. Escobar, M. Leriche, C. Barthe, B. Aouizerats, C. Augros, P. Aumond, F. Auguste, P. Bechtold, S. Berthet, S. Bielli, F. Bosseur, O. Caumont, J.-M. Cohard, J. Colin, F. Couvreux, J. Cuxart, G. Delautier, T. Dauhut, V. Ducrocq, J.-B. Filippi, D. Gazen, O. Geoffroy, F. Gheusi, R. Honnert, J.-P. Lafore, C. Lebeaupin Brossier, Q. Libois, T. Lunet, C. Mari, T. Maric, P. Mascart, M. Mogé, G. Molinié, O. Nuissier, F. Pantillon, P. Peyrillé, J. Pergaud, E. Perraud, J. Pianezze, J.-L. Redelsperger, D. Ricard, E. Richard, S. Riette, Q. Rodier, R. Schoetter, L. Seyfried, J. Stein, K. Suhre, M. Taufour, O. Thouron, S. Turner, A. Verrelle, B. Vié, F. Visentin, V. Vionnet, and P. Wautelet. Overview of the meso-nh model version 5.4 and its applications. *Geoscientific Model Development*, 11(5):1929–1969, 2018. doi: 10.5194/gmd-72811-1929-2018.

W. G. Large and J. M. Caron. Diurnal cycling of sea surface temperature, salinity, and current in the cesm coupled climate model. *Journal of Geophysical Research: Oceans*, 120(5):3711–3729, 2015. doi: https://doi.org/10.1002/2014JC010691.

C. Lebeaupin Brossier, V. Ducrocq, and H. Giordani. Two-way one-dimensional high-resolution air–sea coupled modelling applied to mediterranean heavy rain events. *Quarterly Journal of the Royal Meteorological Society*, 135(638):187–204, 2009. doi: 10.1002/qj.338. URL https://rmets.onlinelibrary.wiley.com/doi/abs/10.1002/qj.338.

Florian Lemarié, Guillaume Samson, Jean-Luc Redelsperger, Hervé Giordani, Théo Brivoal, and Madec Gurvan. A simplified atmospheric boundary layer model for an improved representation of air-sea interactions in eddying oceanic models: implementation and first evaluation in NEMO (v4.0). *Geoscientific Model development*, 2020.

Brian E. Mapes. Water's two height scales: The moist adiabat and the radiative troposphere. *Quarterly Journal of the Royal Meteorological Society*, 127(577):2353–2366, 2001. doi: https://doi.org/10.1002/qj.49712757708.

June Raven Marion. *Providing the best turbulent heat flux estimates from eddy correlation and bulk methods using DYNAMO data*. Oregon State University, October 2014.

Sébastien Masson, Pascal Terray, Gurvan Madec, Jing-Jia Luo, Toshio Yamagata, and Keiko Takahashi. Impact of intra-daily SST variability on ENSO characteristics in a coupled model. *Climate Dynamics*, 39(3-4):681–707, August 2012. doi: https://doi.org/10.1007/s00382-011-1247-2.

Adrian J. Matthews, Dariusz B. Baranowski, Karen J. Heywood, Piotr J. Flatau, and Sunke Schmidtko. The Surface Diurnal Warm Layer in the Indian Ocean during CINDY/DYNAMO. *Journal of Climate*, 27(24):9101–9122, December 2014. doi: https://doi.org/10.1175/JCLI-D-14-00222.1.

Aurélie J. Moulin, James N. Moum, and Emily L. Shroyer. Evolution of Turbulence in the Diurnal Warm Layer. *Journal of Physical Oceanography*, 48(2):383–396, February 2018. doi: https://doi.org/10.1175/JPO-D-17-0170.1.

J. N. Moum. Profiler Measurements of Vertical Velocity Fluctuations in the Ocean. *Journal of Atmospheric and Oceanic Technology*, 7(2):323–333, April 1990. doi: https://doi.org/10.1175/1520-0426(1990)007\textless0323:PMOVVF\textgreater2.0.CO;2.

James N. Moum, Simon P. de Szoeke, William D. Smyth, James B. Edson, H. Langley DeWitt, Aurélie J. Moulin, Elizabeth J. Thompson, Christopher J. Zappa, Steven A. Rutledge, Richard H. Johnson, and Christopher W. Fairall. Air–Sea Interactions from Westerly Wind Bursts During the November 2011 MJO in the Indian Ocean. *Bulletin of the American Meteorological Society*, 95(8):1185–1199, August 2014. doi: https://doi.org/10.1175/BAMS-D-12-00225.1.

J. Carter Ohlmann, David A. Siegel, and Curtis D. Mobley. Ocean Radiant Heating. Part I: Optical Influences. *Journal of Physical Oceanography*, 30(8):1833–1848, August 2000. doi: https://doi.org/10.1175/1520-0485(2000)030\textless1833:ORHPIO\textgreater2.0.CO;2.

Clayton A. Paulson and James J. Simpson. Irradiance Measurements in the Upper Ocean. *Journal of Physical Oceanography*, 7(6):952–956, November 1977. doi: https://doi.org/10.1175/1520-0485(1977)007\textless0952:IMITUO\textgreater2.0.CO;2.

S.B. Pope. *Turbulent Flows*. Cambridge University Press, 2000.

James F. Price, Robert A. Weller, and Robert Pinkel. Diurnal cycling: Observations and models of the upper ocean response to diurnal heating, cooling, and wind mixing. *Journal of Geophysical Research*, 91(C7):8411, 1986. doi: https://doi.org/10.1029/JC091iC07p08411.

David A. Randall, Kuan-Man Xu, Richard J. C. Somerville, and Sam Iacobellis. Single-column models and cloud ensemble models as links between observations and climate models. *Journal of Climate*, 9(8):1683–1697, 1996. doi: http://www.jstor.org/stable/26201368.

J. L. Redelsperger and G. Sommeria. Three-dimensional simulation of a convective storm: Sensitivity studies on subgrid parameterization and spatial resolution. *Journal of the Atmospheric Sciences*, 43(22):2619–2635, 1986. doi: 10.1175/1520-0469(1986)043<2619:TDSOAC>2.0.CO;2.

G. Reffray, R. Bourdalle-Badie, and C. Calone. Modelling turbulent vertical mixing sensitivity using a 1-D version of NEMO. *Geoscientific Model Development*, 8(1):69–86, 2015. doi: https://doi.org/10.5194/gmd-8-69-2015.

Stephan R. Roode, Thomas Frederikse, A. Pier Siebesma, Andrew S. Ackerman, Jan Chylik, Paul R. Field, Jens Fricke, Micha Gryschka, Adrian Hill, Rachel Honnert, Steve K. Krueger, Christine Lac, Andrew T. Lesage, and Lorenzo Tomassini. Turbulent Transport in the Gray Zone: A Large Eddy Model Intercomparison Study of the CONSTRAIN Cold Air Outbreak Case. *Journal of Advances in Modeling Earth Systems*, 11(3):597–623, March 2019. doi: 1https://doi.org/0.1029/2018MS001443.

Angela K. Rowe and Robert A. Houze Jr. Cloud organization and growth during the transition from suppressed to active mjo conditions. *Journal of Geophysical Research: Atmospheres*, 120(19):10,324–10,350, 2015. doi: https://doi.org/10.1002/2014JD022948.

James H. Ruppert and Richard H. Johnson. Diurnally Modulated Cumulus Moistening in the Preonset Stage of the Madden–Julian Oscillation during DYNAMO*. *Journal of the Atmospheric Sciences*, 72(4):1622–1647, April 2015. doi: https://doi.org/10.1175/JAS-D-14-0218.1.

James H. Ruppert and Richard H. Johnson. On the cumulus diurnal cycle over the tropical warm pool. *Journal of Advances in Modeling Earth Systems*, 8(2):669–690, June 2016. doi: https://doi.org/10.1002/2015MS000610.

Irina Sandu and Bjorn Stevens. On the factors modulating the stratocumulus to cumulus transitions. *Journal of the Atmospheric Sciences*, 68(9):1865–1881, 2011. doi: https://doi.org/10.1175/2011JAS3614.1.

Y. Seity, P. Brousseau, S. Malardel, G. Hello, P. Bénard, F. Bouttier, C. Lac, and V. Masson. The AROME-France Convective-Scale Operational Model. *Monthly Weather Review*, 139(3):976–991, March 2011. ISSN 0027-0644, 1520-0493. URL http://journals.ametsoc.org/doi/abs/10.1175/2010MWR3425.1.

Hyodae Seo, Aneesh C. Subramanian, Arthur J. Miller, and Nicholas R. Cavanaugh. Coupled Impacts of the Diurnal Cycle of Sea Surface Temperature on the Madden–Julian Oscillation. *Journal of Climate*, 27(22):8422–8443, 11 2014. ISSN 0894-8755. doi: 10.1175/JCLI-D-14-00141.1. URL https://doi.org/10.1175/JCLI-D-14-00141.1.

Toshiaki Shinoda. Impact of the Diurnal Cycle of Solar Radiation on Intraseasonal SST Variability in the Western Equatorial Pacific. *Journal of Climate*, 18(14):2628–2636, July 2005. doi: https://doi.org/10.1175/JCLI3432.1.

A. Pier Siebesma, Christopher S. Bretherton, Andrew Brown, Andreas Chlond, Joan Cuxart, Peter G. Duynkerke, Hongli Jiang, Marat Khairoutdinov, David Lewellen, Chin-Hoh Moeng, Enrique Sanchez, Bjorn Stevens, and David E. Stevens. A Large Eddy Simulation Intercomparison Study of Shallow Cumulus Convection. *Journal of the Atmospheric Sciences*, 60(10):1201–1219, May 2003. doi: https://doi.org/10.1175/1520-0469(2003)60\textless1201:ALESIS\textgreater2.0.CO;2.

Eric D. Skyllingstad and Simon P. de Szoeke. Cloud-resolving large-eddy simulation of tropical convective development and surface fluxes. *Monthly Weather Review*, 143(7):2441–2458, 2015. doi: https://doi.org/10.1175/MWR-D-14-00247.1.

W. D. Smyth, J. N. Moum, L. Li, and S. A. Thorpe. Diurnal Shear Instability, the Descent of the Surface Shear Layer, and the Deep Cycle of Equatorial Turbulence. *Journal of Physical Oceanography*, 43(11):2432–2455, November 2013. doi: https://doi.org/10.1175/JPO-D-13-089.1.

Adam Sobel, Shuguang Wang, and Daehyun Kim. Moist Static Energy Budget of the MJO during DYNAMO. *Journal of the Atmospheric Sciences*, 71(11):4276–4291, November 2014. doi: https://doi.org/10.1175/JAS-D-14-0052.1.

Adam H. Sobel and Christopher S. Bretherton. Modeling Tropical Precipitation in a Single Column. *Journal of Climate*, 13(24):4378–4392, December 2000. doi: https://doi.org/10.1175/1520-0442(2000)013\textless4378:MTPIAS\textgreater2.0.CO;2.

Adam H. Sobel, Johan Nilsson, and Lorenzo M. Polvani. The Weak Temperature Gradient Approximation and Balanced Tropical Moisture Waves*. *Journal of the Atmospheric Sciences*, 58(23):3650–3665, December 2001. doi: https://doi.org/10.1175/1520-0469(2001)058\textless3650:TWTGAA\textgreater2.0.CO;2.

Alexander Soloviev and Roger Lukas. Observation of large diurnal warming events in the near-surface layer of the western equatorial Pacific warm pool. *Deep Sea Research Part I: Oceanographic Research Papers*, 44(6):1055–1076, June 1997. doi: https://doi.org/10.1016/S0967-0637(96)00124-0.

Alexander Soloviev and Roger Lukas. *The Near-Surface Layer of the Ocean*, volume 48 of *Atmospheric and Oceanographic Sciences Library*. Springer Netherlands, Dordrecht, 2014. doi: 10.1007/978-94-007-7621-0. URL `http://link.springer.com/10.1007/978-94-007-7621-0`.

AV Soloviev. On the vertical structure of the thin surface layer of the ocean during a weak wind. *Izv. Atmos. Oceanic Phys*, 18:579–585, 1982.

Graig Sutherland, Louis Marié, Gilles Reverdin, Kai H. Christensen, Göran Broström, and Brian Ward. Enhanced Turbulence Associated with the Diurnal Jet in the Ocean Surface Boundary Layer. *Journal of Physical Oceanography*, 46(10):3051–3067, October 2016. doi: https://doi.org/10.1175/JPO-D-15-0172.1.

Tetsuya Takemi, Osamu Hirayama, and Changhai Liu. Factors responsible for the vertical development of tropical oceanic cumulus convection. *Geophysical Research Letters*, 31(11), June 2004. doi: https://doi.org/10.1029/2004GL020225.

Zhihong Tan, Tapio Schneider, João Teixeira, and Kyle G. Pressel. Large-eddy simulation of subtropical cloud-topped boundary layers: 1. a forcing framework with closed surface energy balance. *Journal of Advances in Modeling Earth Systems*, 8(4):1565–1585, 2016. doi: https://doi.org/10.1002/2016MS000655.

J. Teixeira, B. Stevens, C. S. Bretherton, R. Cederwall, J. D. Doyle, J. C . Golaz, A. A. M. Holtslag, S. A . Klein, J. K. Lundquist, D. A. Randall, A. P. Siebesma, and P. M. M. Soares. Parameterization of the Atmospheric Boundary Layer: A View from Just Above the Inversion. *Bulletin of the American Meteorological Society*, 89(4):453–458, April 2008. doi: https://doi.org/10.1175/BAMS-89-4-453.

Pascal Terray, Kakitha Kamala, Sébastien Masson, Gurvan Madec, A. K. Sahai, Jing-Jia Luo, and Toshio Yamagata. The role of the intra-daily SST variability in the Indian monsoon variability and monsoon-ENSO–IOD relationships in a global coupled model. *Climate Dynamics*, 39(3-4):729–754, August 2012. doi: https://doi.org/10.1007/s00382-011-1240-9.

Margreet C vanZanten, Bjorn Stevens, Louise Nuijens, A Pier Siebesma, A. S. Ackerman, F. Burnet, A. Cheng, F. Couvreux, H. Jiang, M. Khairoutdinov, Y. Kogan, D. C. Lewellen, D. Mechem, K. Nakamura, A. Noda, B. J. Shipway, J. Slawinska, S. Wang, and A. Wyszogrodzki. Controls on precipitation and cloudiness in simulations of trade–wind cumulus as observed during RICO. *Journal of Advances in Modeling Earth Systems*, 3(2), February 2011. doi: https://doi.org/10.1029/2011MS000056.

Tammy M. Weckwerth, James W. Wilson, and Roger M. Wakimoto. Thermodynamic Variability within the Convective Boundary Layer Due to Horizontal Convective Rolls. *Monthly Weather Review*, 124(5):769–784, May 1996. doi: https://doi.org/10.1175/1520-0493(1996)124\textless0769:TVWTCB\textgreater2.0.CO;2.

S. J. Woolnough, J. M. Slingo, and B. J. Hoskins. The Relationship between Convection and Sea Surface Temperature on Intraseasonal Timescales. *Journal of Climate*, 13(12):2086–2104, June 2000. doi: https://doi.org/10.1175/1520-0442(2000)013\textless2086:TRBCAS\textgreater2.0.CO;2.

Gui-Ying Yang and Julia Slingo. The Diurnal Cycle in the Tropics. *Monthly Weather Review*, 129(4):784–801, April 2001. doi: https://doi.org/10.1175/1520-0493(2001)129<0784:TDCITT>2.0.CO;2.

Kunio Yoneyama, Chidong Zhang, and Charles N. Long. Tracking Pulses of the Madden–Julian Oscillation. *Bulletin of the American Meteorological Society*, 94(12):1871–1891, December 2013. doi: https://doi.org/10.1175/BAMS-D-12-00157.1.

Paquita Zuidema, Zhujun Li, Reginald J. Hill, Ludovic Bariteau, Bob Rilling, Chris Fairall, W. Alan Brewer, Bruce Albrecht, and Jeff Hare. On trade wind cumulus cold pools. *Journal of the Atmospheric Sciences*, 69(1):258–280, 2012. doi: https://doi.org/10.1175/JAS-D-11-0143.1.